Electronic Supplementary Material (ESI) for ChemComm.

Supporting Information

for

Mechanistic insight into initiation and regioselectivity in the copolymerization of epoxides and anhydrides by Al complexes

Yanay Popowski,[a] Juan J. Moreno,[c] Asa W. Nichols,[c] Shelby L. Hooe,[c] Caitlin J. Bouchey,[a,b], Nigam P. Rath,[d] Charles W. Machan,[c,*] and William B. Tolman[a,*]

[a]*Department of Chemistry, Washington University in St. Louis, Campus Box 1134, 1 Brookings Drive, St. Louis, MO 63130, USA.*
[b]*Department of Chemistry, University of Minnesota, 207 Pleasant St. SE, Minneapolis, MN 55455, USA.*
[c]*Department of Chemistry, University of Virginia, PO Box 400319, Charlottesville, VA 22904-4319, USA.*
[d]*Department of Chemistry and Biochemistry and Center for Nanoscience, University of Missouri-St. Louis, One University Boulevard, St. Louis, MO 63121*

Table of Contents

1. Materials, methods, and general considerations **S3**
2. List of complexes **S4**
3. Synthesis and characterization **S4**
3.1. Synthesis of $^{t\text{-Bu}}$dhphenH_2 S4
3.2. Synthesis of ($^{t\text{-Bu}}$dhbpy)AlCl S6
3.3. Synthesis of ($^{t\text{-Bu}}$dhbpy)AlO^{i}Pr S6
3.4. Synthesis of ($^{t\text{-Bu}}$dhphen)AlCl S7
3.5. Synthesis of ($^{t\text{-Bu}}$salph)Al(oCPMA) S7
3.6. Synthesis of ($^{t\text{-Bu}}$salph)Al(oCPCA) S8
3.7. Synthesis of ($^{t\text{-Bu}}$salph)Al(oCHCA) S9
3.8. Synthesis of ($^{t\text{-Bu}}$salph)Al(oTMPA) S9
4. NMR spectra **S11**

Figure S1. ^{1}H NMR of $^{t\text{-Bu}}$dhphenH_2 S11
Figure S2. ^{13}C{^{1}H} NMR of $^{t\text{-Bu}}$dhphenH_2 S12
Figure S3. ^{1}H NMR of ($^{t\text{-Bu}}$dhbpy)AlCl S12
Figure S4. ^{13}C{^{1}H} NMR of ($^{t\text{-Bu}}$dhbpy)AlCl S13
Figure S5. ^{1}H NMR of ($^{t\text{-Bu}}$dhphen)AlCl S13
Figure S6. ^{13}C{^{1}H} NMR of ($^{t\text{-Bu}}$dhphen)AlCl S14
Figure S7. ^{1}H NMR of ($^{t\text{-Bu}}$dhbpy)AlO^{i}Pr S14
Figure S8. ^{13}C{^{1}H} NMR of ($^{t\text{-Bu}}$dhbpy)AlO^{i}Pr S15
Figure S9. ^{1}H NMR of ($^{t\text{-Bu}}$salph)Al(oCPMA) S15
Figure S10. ^{13}C{^{1}H} NMR of ($^{t\text{-Bu}}$salph)Al(oCPMA) S16

Figure S11. ^{1}H NMR spectrum of the ring-opening of CPCA by ($^{t\text{-Bu}}$salph)AlO^{i}Pr S16
Figure S12. ^{13}C{^{1}H} NMR spectrum of the ring-opening of CPCA by ($^{t\text{-Bu}}$salph)AlO^{i}Pr S17
Figure S13. ^{1}H-^{13}C HMBC spectrum of the ring-opening of CPCA by ($^{t\text{-Bu}}$salph)AlO^{i}Pr S17
Figure S14. ^{1}H NMR spectrum of the ring-opening of CHCA by ($^{t\text{-Bu}}$salph)AlO^{i}Pr S18
Figure S15. ^{13}C{^{1}H} NMR spectrum of the ring-opening of CHCA by ($^{t\text{-Bu}}$salph)AlO^{i}Pr S18
Figure S16. ^{1}H-^{13}C HMBC spectrum of the ring-opening of CHCA by ($^{t\text{-Bu}}$salph)AlO^{i}Pr S19
Figure S17. ^{1}H NMR spectrum of the ring-opening of TPMA by ($^{t\text{-Bu}}$salph)AlO^{i}Pr S19
Figure S18. ^{13}C{^{1}H} NMR spectrum of the ring-opening of TPMA by ($^{t\text{-Bu}}$salph)AlO^{i}Pr S20
Figure S19. ^{1}H-^{13}C HMBC spectrum of the ring-opening of TPMA by ($^{t\text{-Bu}}$salph)AlO^{i}Pr S20
5. General polymerization procedure **S22**
6. Stoichiometric reactions of CPMA ring-opening monitored by NMR **S22**
Table S1. Conversion (%) of CPMA ring-opening by the ($^{t\text{-Bu}}$salph)AlO^{i}Pr and ($^{t\text{-Bu}}$dhbpy)AlO^{i}Pr complexes S23
Figure S20. ^{1}H NMR monitoring of CPMA ring-opening by ($^{t\text{-Bu}}$salph)AlO^{i}Pr S23
Figure S21. ^{1}H NMR monitoring of CPMA ring-opening by ($^{t\text{-Bu}}$dhbpy)AlO^{i}Pr S24
7. Temperature dependence of CPMA ring-opening **S24**
Table S2. Conversion (%) of CPMA ring-opening by ($^{t\text{-Bu}}$salph)AlO^{i}Pr at 80 °C S24
8. Kinetics measurements of CPMA ring-opening by NMR **S25**
Figure S22. Representative ^{1}H NMR spectral array for ring-opening of CPMA S26
9. Kinetic data analysis **S26**
Table S3. Summary of kinetic parameters S28
Figure S23. Representative plots of [($^{t\text{-Bu}}$salph)AlO^{i}Pr] decay as a function of time S29
Figure S24. Plots of the average k_{obs} values calculated for the ring-opening of CPMA S29
10. Evaluation of equilibrium in the ring-opening process **S30**
Figure S25. ^{1}H NMR monitoring of the reaction between ($^{t\text{-Bu}}$salph)Al(oCPMA) and CPCA S30
11. X-ray crystallography **S31**
Figure S26. Representation of the X-ray crystal structure of (salph)Al(oCHCA-OiPr) S32
12. References **S32**

1. Materials, methods, and general considerations

All reactions containing either air- and/or water-sensitive compounds were performed within the inert atmosphere of a nitrogen-filled glovebox or using Schlenk line techniques. All reagents were purchased from commercial sources and were used as received, unless otherwise noted. Butylene oxide (BO, 99%, Aldrich) was stirred over calcium hydride for three days, degassed by three freeze-pump-thaw cycles, vacuum transferred to an oven-dried Straus flask, and stored in a glove box under a nitrogen atmosphere. Carbic anhydride (CPMA; Acros >99%) was recrystallized from EtOAc and then sublimed at 80 °C under dynamic vacuum and stored in a glove box under a nitrogen atmosphere. Bis(triphenylphosphine)iminium chloride (PPNCl, 97%, Aldrich) was recrystallized by layering a saturated CH_2Cl_2 solution with dry Et_2O. The crystals obtained were ground into a fine powder and then dried at 60 °C under vacuum prior to transferring and storing in a glove box under a nitrogen atmosphere. The non-symmetric cyclic anhydrides CPCA, CHCA and TPMA were synthesized according to previously-reported procedures.[1-3] The compounds $^{t\text{-Bu}}$dhbpyH$_2$,[4,5] ($^{t\text{-Bu}}$salph)AlCl,[6] and ($^{t\text{-Bu}}$salph)AlO^{i}Pr[7] were prepared as reported previously. Solvents were degassed and passed through a solvent purification system (Glass Contour, Laguna, CA) prior to use, with the exception of deuterated solvents, which were purchased from Cambridge Isotope Laboratories, Inc. and stored in a glovebox over 4 Å molecular sieves prior to use. Nuclear magnetic resonance (NMR) spectroscopy experiments were performed with a Varian Unity Inova (500 MHz) spectrometer. Chemical shifts for ^{1}H and ^{13}C NMR spectra were referenced to residual protium in the deuterated solvent (for ^{1}H NMR) and the deuterated solvent itself (for ^{13}C NMR). Elemental analyses were performed by Galbraith Laboratories Inc. in Knoxville,

TN. X-ray diffraction measurements were collected with Mo Kα or Cu Kα source and a Bruker X8 diffractometer equipped with a Kappa Apex II CCD using a graphite monochromator and an Oxford Cryostream LT device. Apex III and SAINT software packages[8] were used for data collection and data integration. Structure solutions were performed with SHELXT[9] or SHELXS[10] using OLEX[11] or ShelXle[12] as graphical interfaces. The structures were refined against F2 on all data by full matrix least squares with SHELXL.[10]

2. List of complexes

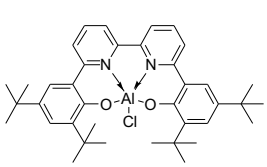

($^{t\text{-Bu}}$dhbpy)AlCl

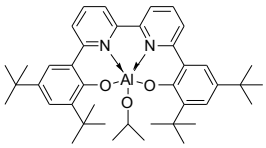

($^{t\text{-Bu}}$dhbpy)AlO^{i}Pr

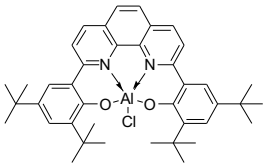

($^{t\text{-Bu}}$dhphen)AlCl

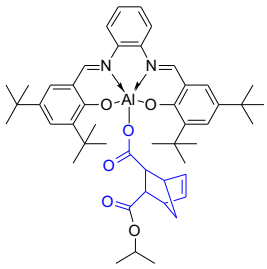

($^{t\text{-Bu}}$salph)Al(oCPMA)

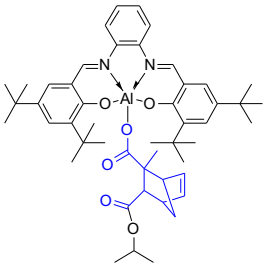

($^{t\text{-Bu}}$salph)Al(oCPCA)

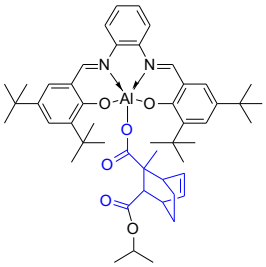

($^{t\text{-Bu}}$salph)Al(oCHCA)

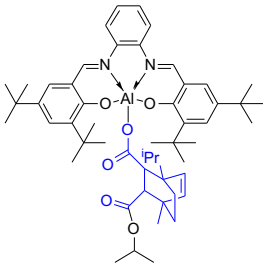

($^{t\text{-Bu}}$salph)Al(oTPMA)

3. Synthesis and characterization

3.1. Synthesis of $^{t\text{-Bu}}$dhphenH$_2$. A Schlenk flask (500 mL) with stir bar was charged with 2-bromo-4,6-di-tert-butyl-phenol (5.00 g, 0.0175 mol) and dry diethyl ether (200 mL). The resulting solution was cooled to −78 °C under N_2 using a dry ice/acetone ice bath. After 10 min, n-butyllithium (2.5 M in hexanes) was added slowly via syringe (16.0 mL, 0.040 mol), after which the solution was allowed to warm to room temperature with vigorous

stirring for 2 h. The solution was again chilled to −78 °C and trimethyl borate was added rapidly by syringe (3.15 mL, 0.0283 mol) with vigorous stirring and left for 10 min. The cooling bath was then removed and the mixture stirred overnight at room temperature under N_2 (16 h). After this time, the flask was cooled to 0 °C before quenching with HCl (25 mL, 2 M) and opened to air. The resulting suspension was separated into organic and aqueous layers, and the aqueous layer was extracted with CH_2Cl_2 (3 × 50 mL). A yellow oil was isolated and used without further purification.

A microwave-assisted Suzuki-Miyaura coupling reaction was performed with 2,9-dichloro-1,10-phenanthroline and the crude boronic acid generated above using an Anton Paar Multiwave Pro equipped with an 8NXF100 Rotor. Two PTFE reaction tubes were each equipped with a magnetic stir bar, charged with Na_2CO_3 (2.78 g, 26.3 mmol), and moved inside a N_2-filled glovebox. Separate Schlenk flasks were prepared with Ar-degassed deionized water and methanol and also brought into the N_2-filled glovebox. $Pd(PPh_3)_4$ (0.18 g, 0.16 mmol) and 2,9-dichloro-1,10-phenanthroline (0.75 g, 3.0 mmol) were added to each PTFE reaction tube. The boronic acid was added in the glovebox by diluting the oil in toluene (20 mL total volume) and splitting this stock solution equally between the two PTFE vessels. Methanol (10 mL), deionized water (10 mL), and toluene (30 mL) were added to the vessels. The vessels were sealed, and loaded into the microwave. The temperature was brought to 170°C as fast as possible and held for 90 min. The temperature was monitored using the Anton Parr TProbe-S in a quartz immersion tube in a vessel containing only the biphasic solvent mixture and was controlled via the built-in temperature control feature. After cooling to room temperature, the reaction solutions in each of the tubes were combined, and the organic and aqueous

layers were separated. The aqueous layer was diluted with 50 mL brine and extracted with CH_2Cl_2 (6 x 50 mL) and all organic fractions were combined, dried with $MgSO_4$, and filtered. The isolated solid was washed with boiling chloroform to remove any residual organic fraction, and all organic layers were combined and condensed under vacuum to yield a crystalline yellow solid once approximately 50 mL of solvent remained. This suspension was chilled to 0°C for 1 h and the pure solid was collected by vacuum filtration. Yield 2.50 g, 70%. ^{1}H NMR ($CDCl_3$, 500 MHz, 25 ºC): δ 8.37 (d, *J* = 8.7 Hz, 2H), 8.29 (d, *J* = 8.7 Hz, 2H), 7.84 (d, *J* = 2.4 Hz, 2H), 7.81 (s, 2H), 7.51 (d, *J* = 2.4 Hz, 2H), 1.58 (s, 18H), 1.42 (s, 18H). ^{13}C{^{1}H} ($CDCl_3$, 126 MHz, 25 ºC): δ 159.8, 157.6, 142.3, 140.11, 138.4, 137.6, 127.4, 127.2, 126.0, 122.0, 121.0, 118.9, 35.8, 34.6, 31.9, 30.2. ESI-HRMS: Calculated m/z for $C_{40}H_{48}N_2O_2$ $[M+H]^+$ = 589.3794 found = 589.3891.

3.2. Synthesis of ($^{t\text{-Bu}}$dhbpy)AlCl. In a glovebox, a 1.78 M solution of Et_2AlCl in toluene (71 µL, 0.13 mmol) was added dropwise to a solution of $^{t\text{-Bu}}$dhbpyH_2 (72 mg, 0.13 mmol) in CH_2Cl_2 (3 mL). The reaction was allowed to stir for 24 h at room temperature, followed by removal of the solvent and drying of the yellow solid obtained under reduced pressure (80 mg, 100% yield). Crystals suitable for X-ray diffraction were grown in a freezer by layering a CH_2Cl_2 solution of the complex with pentane. ^{1}H NMR (500 MHz, CD_2Cl_2) δ 8.13 – 8.05 (m, 4H), 8.00 (dd, *J* = 7.3, 1.4 Hz, 2H), 7.68 (d, *J* = 2.5 Hz, 2H), 7.60 (d, *J* = 2.5 Hz, 2H), 1.60 (s, 18H), 1.40 (s, 18H). ^{13}C{^{1}H} NMR (126 MHz, CD_2Cl_2) δ 159.4, 159.1, 141.4, 140.7, 139.3, 129.1, 125.0, 121.8, 118.4, 117.00, 35.8, 34.2, 31.2, 30.1. ESI-HRMS: Calculated m/z for $C_{38}H_{46}N_2O_2Al$ $[M-Cl]^+$ = 589.3375 found = 589.3427. Anal. Calcd for $C_{38}H_{46}N_2O_2Al$: C, 73.00; H, 7.42; N, 4.48. Found: C, 67.58; H, 7.20; N, 4.16. Since the carbon content is lower than expected we hypothesize that inefficient

combustion is responsible for the result. Nevertheless, based on the additional characterization data, we are confident about the identity and purity of the compound.

3.3. Synthesis of ($^{t\text{-Bu}}$dhbpy)AlO^{i}Pr. In a glovebox, a pressure tube was charged with a magnetic stir bar, $^{t\text{-Bu}}$dhbpyH$_2$ (56.4 mg, 0.0997 mmol), Al(O^{i}Pr)$_3$ (20.4 mg, 0.0997 mmol) and toluene (3 mL). The tube was sealed, brought out of the box and the heterogeneous mixture was stirred overnight at 100 °C, resulting in a clear orange solution. The reaction mixture was cooled to room temperature, brought back into the glovebox and transferred to a vial. The solvent was removed under reduced pressure and the yellow solid obtained was dried under vacuum (65 mg, 100% yield). ^{1}H NMR (500 MHz, CD_2Cl_2) δ 8.04 (dd, *J* = 8.3, 1.4 Hz, 2H), 7.99 (t, *J* = 7.8 Hz, 2H), 7.95 (dd, *J* = 7.5, 1.4 Hz, 2H), 7.63 (d, *J* = 2.5 Hz, 2H), 7.56 (d, *J* = 2.5 Hz, 2H), 3.50 (hept, *J* = 6.0 Hz, 1H), 1.62 (s, 18H), 1.39 (s, 18H), 0.45 (d, *J* = 6.0 Hz, 6H). ^{13}C{^{1}H} NMR (126 MHz, CD_2Cl_2) δ 161.2, 159.9, 147.6, 141.7, 140.6, 138.9, 123.0, 124.9, 122.4, 119.2, 117.3, 63.0, 36.4, 34.7, 31.9, 30.8, 27.4. ESI-HRMS: Calculated m/z for $C_{41}H_{53}N_2O_3Al$ [M-O^{i}Pr]$^{+}$ = 589.3375 found = 589.3427. Anal. Calcd for $C_{41}H_{53}N_2O_3Al$: C, 74.00; H, 7.14; N, 4.31. Found: C, 71.11; H, 7.07; N, 4.29. Similarly to the chloro complex, we believe that the carbon content is lower than expected due to inefficient combustion.

3.4. Synthesis of ($^{t\text{-Bu}}$dhphen)AlCl. The complex was prepared according to the above described procedure for **($^{t\text{-Bu}}$dhbpy)AlCl** from a 1.78 M solution of Et_2AlCl in toluene (61 µL, 0.11 mmol) and $^{t\text{-Bu}}$dhphenH$_2$ (64 mg, 0.11 mmol), and was obtained as an orange solid (71 mg, 100% yield). ^{1}H NMR (500 MHz, $CDCl_3$) δ 8.30 (d, *J* = 8.8 Hz, 4H), 7.81 – 7.74 (m, 4H), 7.67 (d, *J* = 2.4 Hz, 2H), 1.71 (s, 9H), 1.41 (s, 9H). ^{13}C{^{1}H} NMR (126 MHz, $CDCl_3$) δ 161.3, 158.5, 142.4, 139.3, 138.6, 137.5, 130.4, 125.2, 124.7, 123.5, 121.9,

118.1, 36.3, 34.5, 31.7, 30.5. ESI-HRMS: Calculated m/z for $C_{40}H_{46}N_2O_2Al$ $[M\text{-}Cl]^+$ = 613.3375 found = 613.3367. Anal. Calcd for $C_{41}H_{53}N_2O_3Al$: C, 75.89; H, 8.23; N, 4.32. Found: C, 74.69; H, 8.06; N, 4.39. Similarly to the bpy complexes, we believe that the carbon content is lower than expected due to inefficient combustion.

3.5. Synthesis of ($^{t\text{-}Bu}$salph)Al(oCPMA). In a glovebox, a pressure tube was charged with a magnetic stir bar, ($^{t\text{-}Bu}$salph)AlO^iPr (80.0 mg, 0.128 mmol), CPMA (21.0 mg, 0.128 mmol) and dichloroethane (DCE; 3 mL). The tube was sealed, brought out of the box and the heterogeneous mixture was stirred for 3 days at 100 °C. The reaction mixture was then cooled to room temperature, brought back into the box and transferred to a vial. The solvent was removed under reduced pressure and the orange oil was triturated with pentane. The yellow solid obtained was further washed with pentane and dried under vacuo (64 mg, 45% yield). Crystals suitable for X-ray diffraction were grown in a freezer at −30 °C by layering a $CDCl_3$ solution of the complex with pentane. ^{1}H NMR (500 MHz, $CDCl_3$) δ 8.95 (s, 1H), 8.94 (s, 1H), 7.73 (dd, *J* = 6.1, 3.5 Hz, 2H), 7.64 (t, *J* = 2.5 Hz, 2H), 7.37 (dt, *J* = 6.2, 3.7 Hz, 2H), 7.25 – 7.20 (m, 2H), 6.03 (dd, *J* = 5.6, 2.9 Hz, 1H), 5.40 (dd, *J* = 5.7, 2.9 Hz, 1H), 4.50 (hept, *J* = 6.4 Hz, 1H), 2.96 (dd, *J* = 10.2, 3.5 Hz, 1H), 2.82 (s, 1H), 2.76 – 2.69 (m, 2H), 1.60 (s, 9H), 1.60 (s, 9H), 1.35 (s, 9H), 1.35 (s, 9H), 1.13 (dt, *J* = 8.4, 2.0 Hz, 1H), 1.00 (d, *J* = 8.3 Hz, 1H), 0.94 (d, *J* = 6.3 Hz, 3H), 0.59 (d, *J* = 6.3 Hz, 3H). ^{13}C{^{1}H} NMR (126 MHz, $CDCl_3$) δ 173.1, 172.8, 164.7, 164.7, 162.9, 162.7, 141.3, 141.2, 139.2, 139.2, 138.7, 138.5, 135.0, 134.2, 132.6, 132.5, 128.4, 128.2, 128.0, 127.9, 118.8, 118.7, 115.6, 115.4, 66.7, 50.6, 48.5, 48.0, 47.0, 45.7, 35.8, 34.2, 31.5, 30.0, 29.9, 22.0, 21.3. ESI-HRMS: Calculated m/z for $C_{48}H_{61}N_2O_6Al$ $[M+H]^+$ = 789.4423 found = 789.4504.

3.6. Synthesis of ($^{t\text{-Bu}}$salph)Al(oCPCA). In a glove box ($^{t\text{-Bu}}$salph)AlO^{i}Pr (12.6 mg, 20.1 μmol, 1 eq.) and CPCA (18.0 mg, 0.101 mmol, 5 eq.) were dissolved in 0.5 mL of $CDCl_3$ and added into a J-Young NMR tube. The tube was brought out of the box and placed in an oil bath at 60 °C. The progress of the reaction was monitored by ^{1}H NMR spectroscopy over 8 days until the complete conversion of the starting complex. Crystals suitable for X-ray diffraction were grown in a freezer at −30 °C by layering a CH_2Cl_2 solution of the stoichiometric reaction between ($^{t\text{-Bu}}$salph)AlO^{i}Pr and CPCA with pentane. We note that despite a similar conversion to the ring-opening of CPMA were observed within the first 22 h (44% conv), a considerable decrease in rate was noticed after prolonged reaction time (47%, 57% and 67% conversion after 48 h, 70 h and 6 days, respectively) requiring use of excess anhydride in order to achieve complete anhydride ring-opening. ^{1}H NMR (500 MHz, $CDCl_3$) δ 8.93 (s, 1H), 8.92 (s, 1H), 7.72 (dt, *J* = 6.2, 3.0 Hz, 2H), 7.64 (d, *J* = 2.6 Hz, 1H), 7.61 (d, *J* = 2.5 Hz, 1H), 7.36 (dd, *J* = 6.2, 3.3 Hz, 2H), 7.23 (d, *J* = 2.6 Hz, 1H), 7.20 (d, *J* = 2.5 Hz, 1H), 5.95 (dd, *J* = 5.6, 3.0 Hz, 1H), 5.29 (dd, *J* = 5.6, 2.9 Hz, 1H), 4.78 – 4.34 (sept, *J* = 6.2 Hz, 1H), 2.71 (s, 1H), 2.34 – 2.29 (m, 3H), 1.59 (s, 9H), 1.58 (s, 9H), 1.35 (s, 9H), 1.33 (s, 9H), 1.28 – 1.25 (m, 1H), 1.12 – 1.08 (m, 1H), 0.96 (d, *J* = 6.3 Hz, 1H), 0.61 (d, *J* = 6.3 Hz, 1H). ^{13}C{^{1}H} NMR (126 MHz, $CDCl_3$) δ 174.53, 174.06, 164.75, 164.60, 162.81, 162.67, 141.27, 141.16, 139.19, 139.03, 138.62, 138.56, 135.59, 135.34, 132.46, 132.40, 128.22, 128.16, 127.90, 127.90, 118.87, 118.73, 115.50, 115.44, 66.51, 57.11, 55.69, 52.64, 45.91, 45.66, 35.79, 35.75, 34.22, 34.19, 31.43, 29.95, 29.94, 27.19, 22.10, 21.42. ESI-HRMS: Calculated m/z for $C_{49}H_{63}N_2O_6Al$ $[M+H]^+$ = 803.4579; found = 803.4534.

3.7. Synthesis of ($^{t\text{-Bu}}$salph)Al(oCHCA). The complex was prepared according to the above described procedure for **($^{t\text{-Bu}}$salph)Al(oCPCA)** with CHCA (19.4 mg, 0.101 mmol, 5 eq.). Crystals suitable for X-ray diffraction were grown in a freezer at −30 °C by layering a CH_2Cl_2 solution of the stoichiometric reaction between ($^{t\text{-Bu}}$salph)AlO^iPr and CHCA with pentane. ^{1}H NMR (500 MHz, $CDCl_3$) δ 8.93 (s, 1H), 8.93 (s, 1H), 7.71 (m, 2H), 7.62 (dd, *J* = 12.3, 2.5 Hz, 2H), 7.39 – 7.33 (m, 2H), 7.22 (dd, *J* = 14.0, 2.6 Hz, 2H), 5.83 (t, *J* = 7.3 Hz, 1H), 5.37 (t, *J* = 7.4 Hz, 1H), 4.45 (sept, *J* = 6.4 Hz, 1H), 2.57 – 2.50 (m, 1H), 2.26 – 2.19 (m, 1H), 1.90 (s, 1H), 1.59 (s, 9H), 1.58 (s, 9H), 1.35 (s, 9H), 1.35 (s, 9H), 1.01 – 0.95 (m, 1H), 0.93 (d, *J* = 6.3 Hz, 1H), 0.87 (m, 1H), 0.56 (d, *J* = 6.3 Hz, 1H). ^{13}C{^{1}H} NMR (126 MHz, $CDCl_3$) δ 174.97, 174.75, 164.69, 164.60, 162.85, 162.63, 141.21, 141.14, 139.18, 139.03, 138.62, 138.55, 133.70, 132.39, 131.86, 128.26, 128.20, 127.87, 127.83, 118.85, 118.78, 115.47, 66.50, 54.74, 53.28, 39.57, 35.79, 35.75, 34.22, 34.19, 32.34, 31.44, 31.41, 30.05, 29.95, 29.94, 26.41, 25.70, 22.08, 21.34, 18.76. ESI-HRMS: Calculated m/z for $C_{50}H_{65}N_2O_6Al$ $[M+H]^+$ = 817.4736; found = 817.4688.

3.8. Synthesis of ($^{t\text{-Bu}}$salph)Al(oTPMA). The complex was prepared according to the above described procedure for **($^{t\text{-Bu}}$salph)Al(oCPCA)** with TPMA (23.6 mg, 0.101 mmol, 5 eq.). ^{1}H NMR (500 MHz, $CDCl_3$) δ 9.02 (s, 1H), 8.98 (s, 1H), 7.79 (m, *J* = 6.5, 3.3 Hz, 2H), 7.67 (d, *J* = 2.5 Hz, 1H), 7.63 (d, *J* = 2.5 Hz, 1H), 7.40 (dd, *J* = 6.2, 3.2 Hz, 2H), 7.28 (m, 1H), 7.23 (d, *J* = 2.6 Hz, 1H), 5.39 (d, *J* = 8.3 Hz, 1H), 5.31 (d, *J* = 8.3 Hz, 1H), 3.94 (sept, *J* = 6.2 Hz, 1H), 2.76 (d, *J* = 11.1 Hz, 1H), 2.48 (d, *J* = 11.6 Hz, 1H), 1.80 (sept, *J* = 6.9 Hz, 1H), 1.61 (s, 9H), 1.60 (s, 9H), 1.37 (s, 9H), 1.35 (s, 9H), 0.96 (s, 3H), 0.89 (m, 3H), 0.86 (d, *J* = 6.2 Hz, 3H), 0.84 – 0.76 (m, 1H), 0.57 (d, *J* = 6.3 Hz, 3H), 0.52 (d, *J* = 6.9 Hz, 3H), 0.47 (d, *J* = 6.8 Hz, 3H). ^{13}C{^{1}H} NMR (126 MHz, $CDCl_3$) δ 172.39, 171.43,

164.63, 164.47, 162.62, 162.51, 141.46, 139.21, 139.20, 138.79, 138.56, 135.61, 134.45, 132.46, 132.42, 128.19, 128.12, 127.72, 127.68, 119.03, 118.78, 115.53, 115.14, 77.41, 77.16, 76.91, 66.38, 56.24, 56.00, 42.55, 35.82, 35.80, 35.33, 35.07, 34.22, 34.20, 31.45, 31.42, 30.21, 30.12, 29.99, 23.05, 22.61, 21.95, 21.34, 18.97, 16.46. ESI-HRMS: Calculated m/z for $C_{50}H_{65}N_2O_6Al$ $[M+H]^+$ = 859.5206; found = 852.5248.

4. NMR spectra

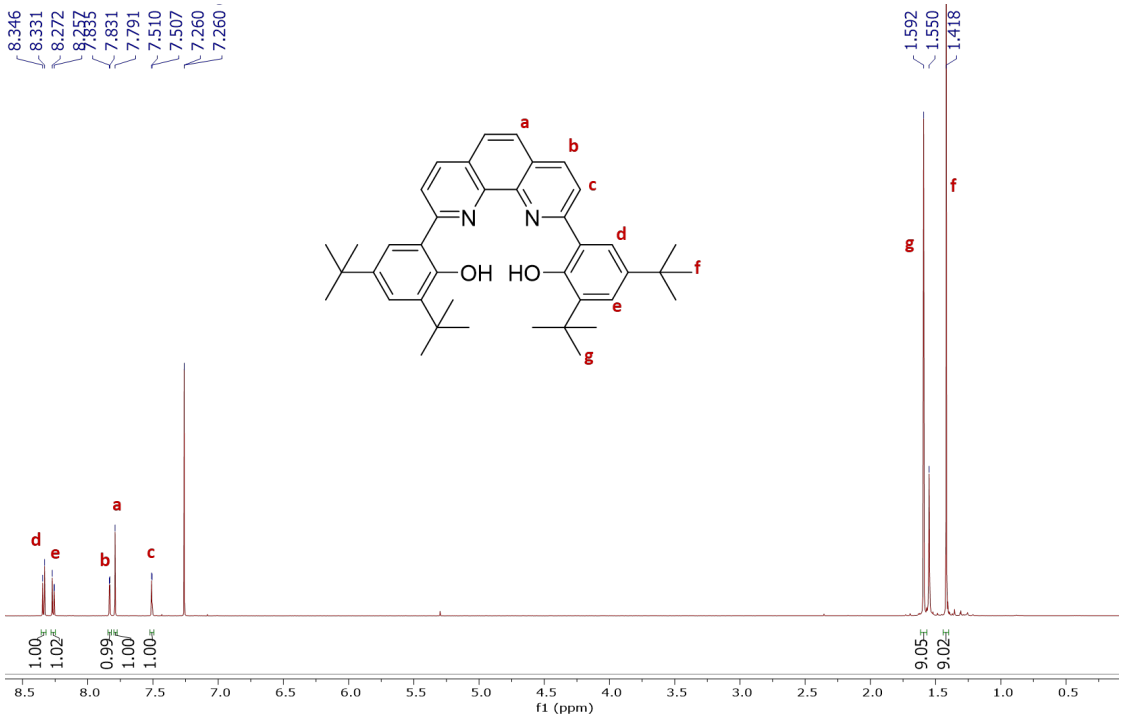

Figure S1. ^{1}H NMR spectrum of $^{t\text{-Bu}}$dhphenH_2 ($CDCl_3$; 500 MHz) with assignments indicated.

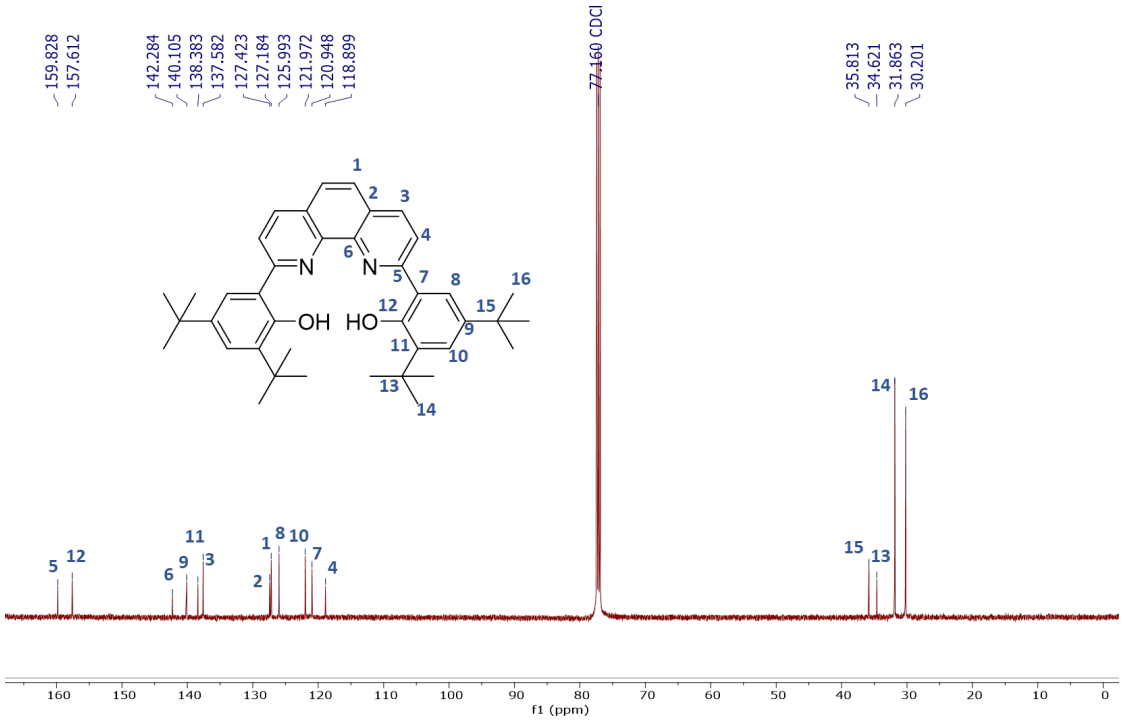

Figure S2. $^{13}C\{^{1}H\}$ NMR spectrum of ($^{t\text{-Bu}}$dhphen) ($CDCl_3$; 126 MHz) with assignments indicated.

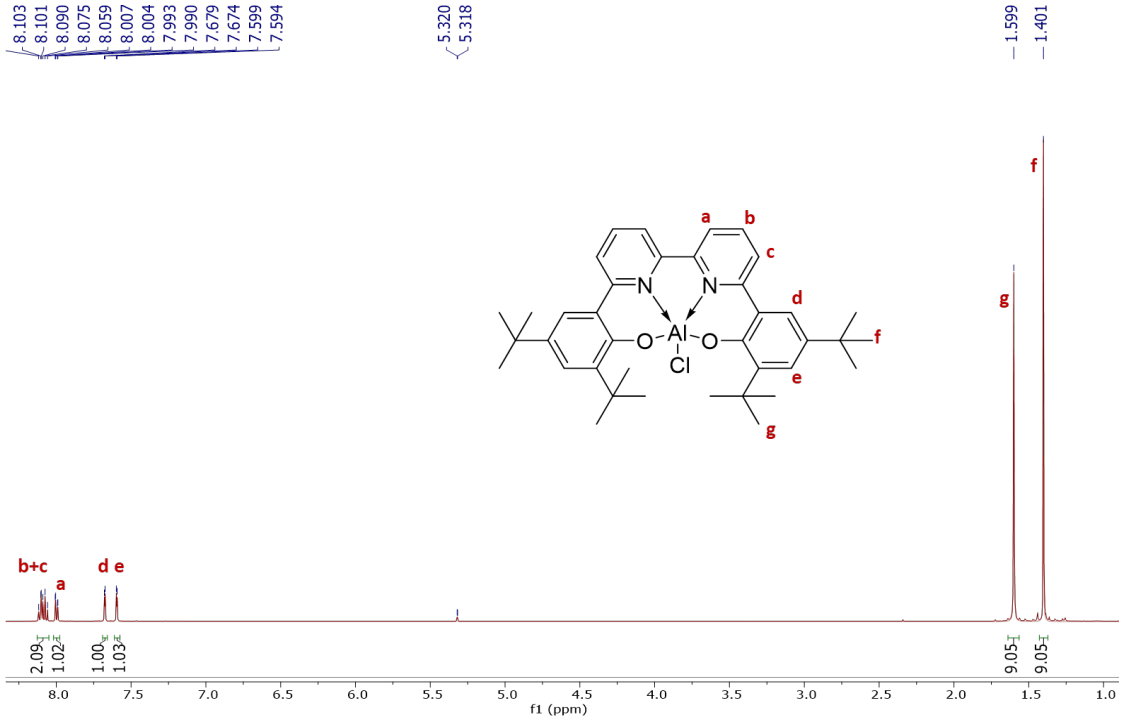

Figure S3. ^{1}H NMR spectrum of ($^{t\text{-Bu}}$dhbpy)AlCl (CD_2Cl_2; 500 MHz) with assignments indicated.

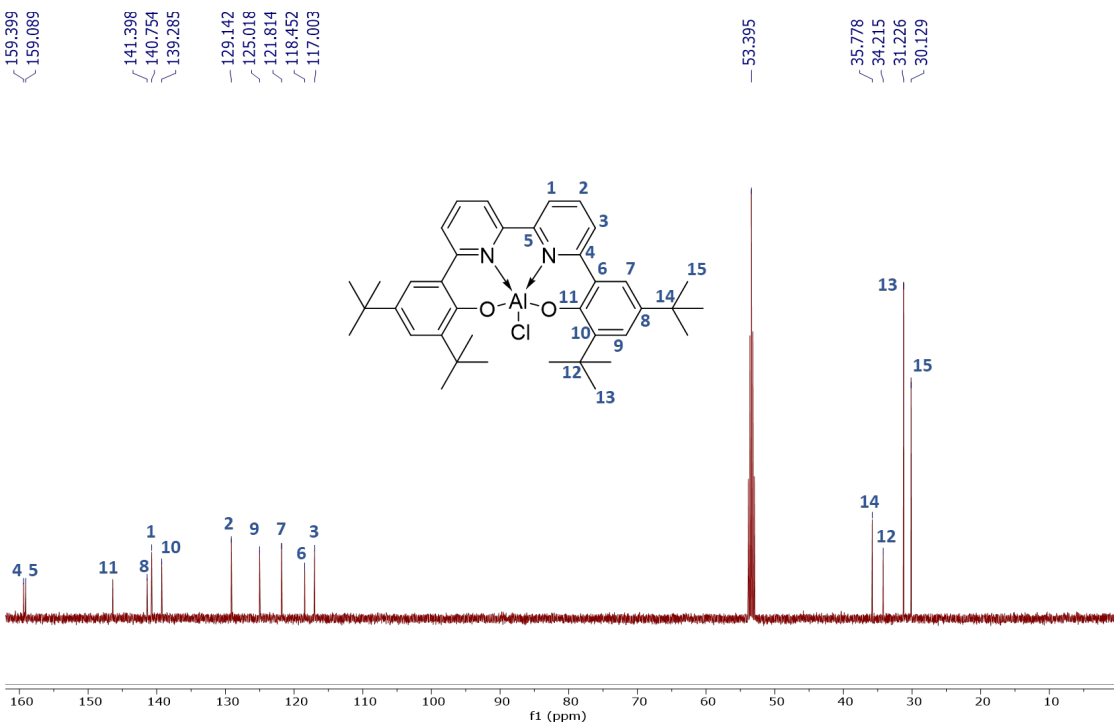

Figure S4. $^{13}C\{^{1}H\}$ NMR spectrum of ($^{t\text{-Bu}}$dhbpy)AlCl (CD_2Cl_2; 126 MHz) with assignments indicated.

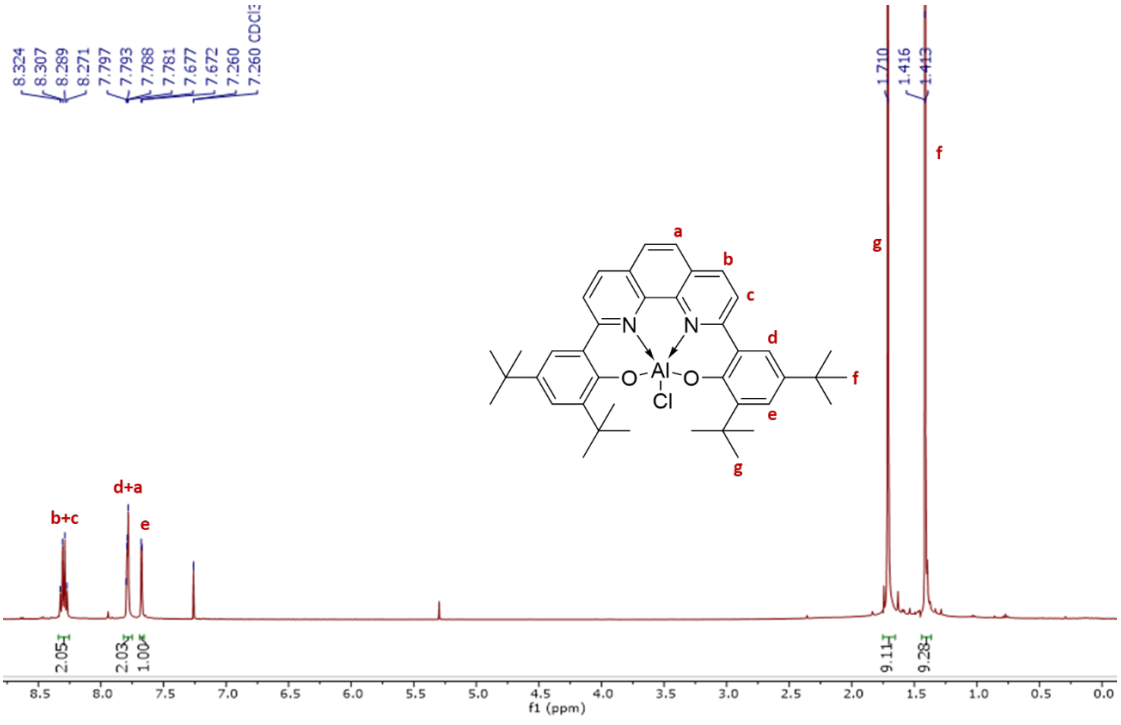

Figure S5. ^{1}H NMR spectrum of ($^{t\text{-Bu}}$dhphen)AlCl ($CDCl_3$; 500 MHz) with assignments indicated.

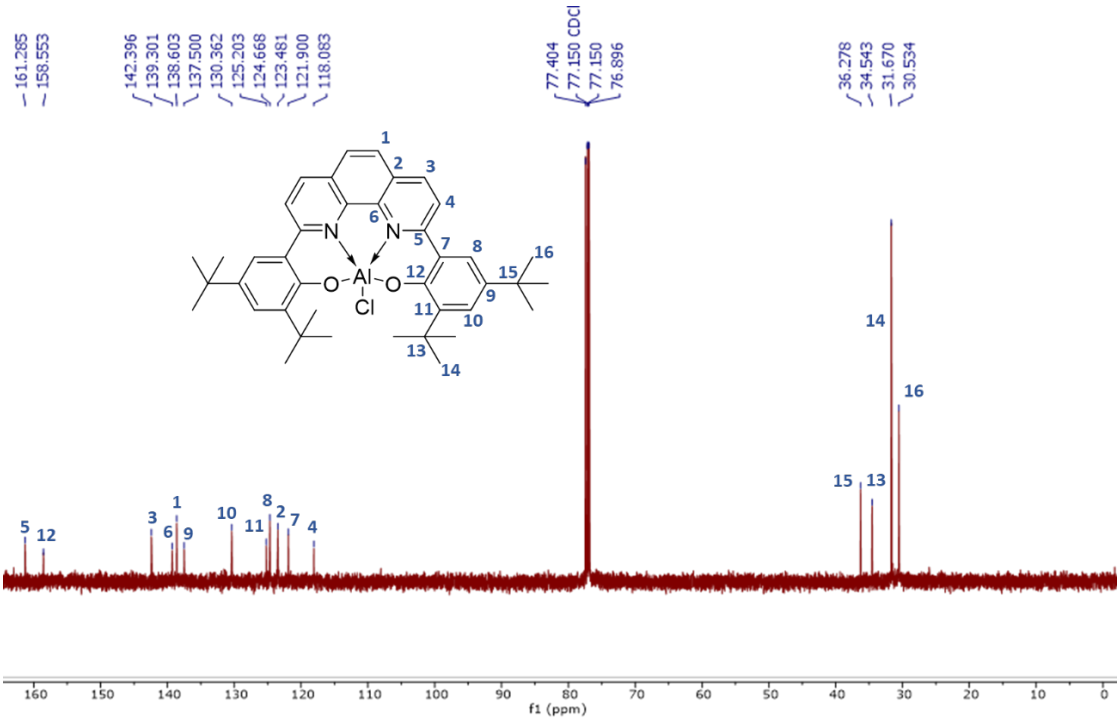

Figure S6. $^{13}C\{^{1}H\}$ NMR spectrum of ($^{t\text{-Bu}}$dhphen)AlCl ($CDCl_3$; 126 MHz) with assignments indicated.

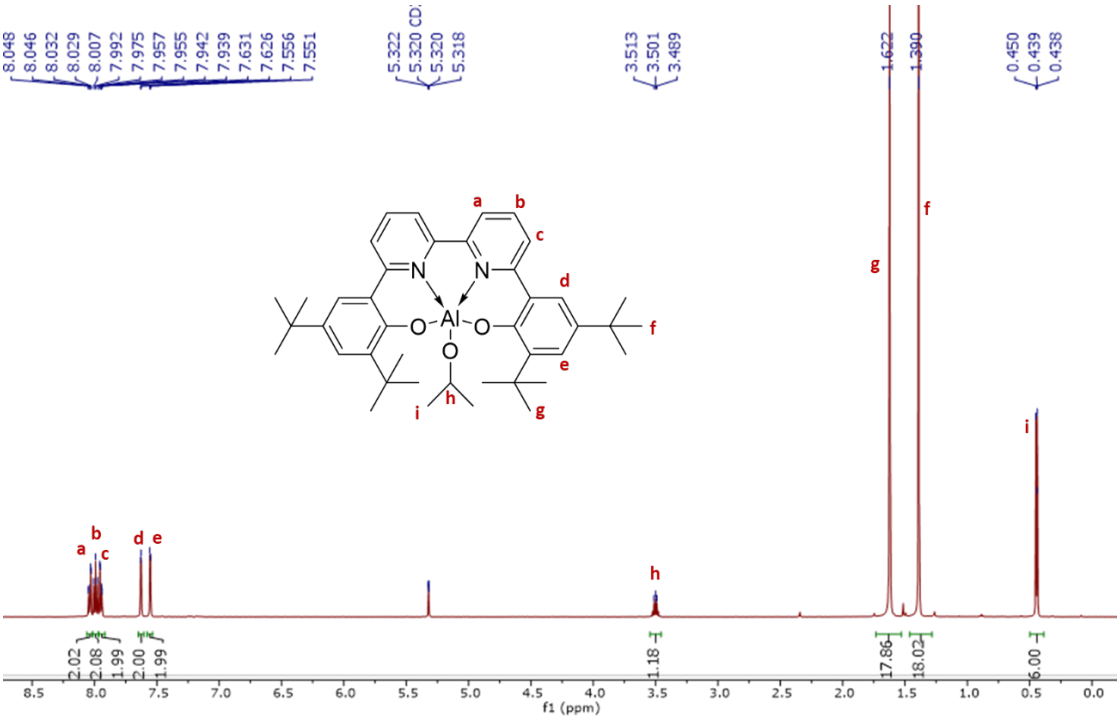

Figure S7. ^{1}H NMR spectrum of ($^{t\text{-Bu}}$dhbpy)AlO^{i}Pr (CD_2Cl_2; 500 MHz) with assignments indicated.

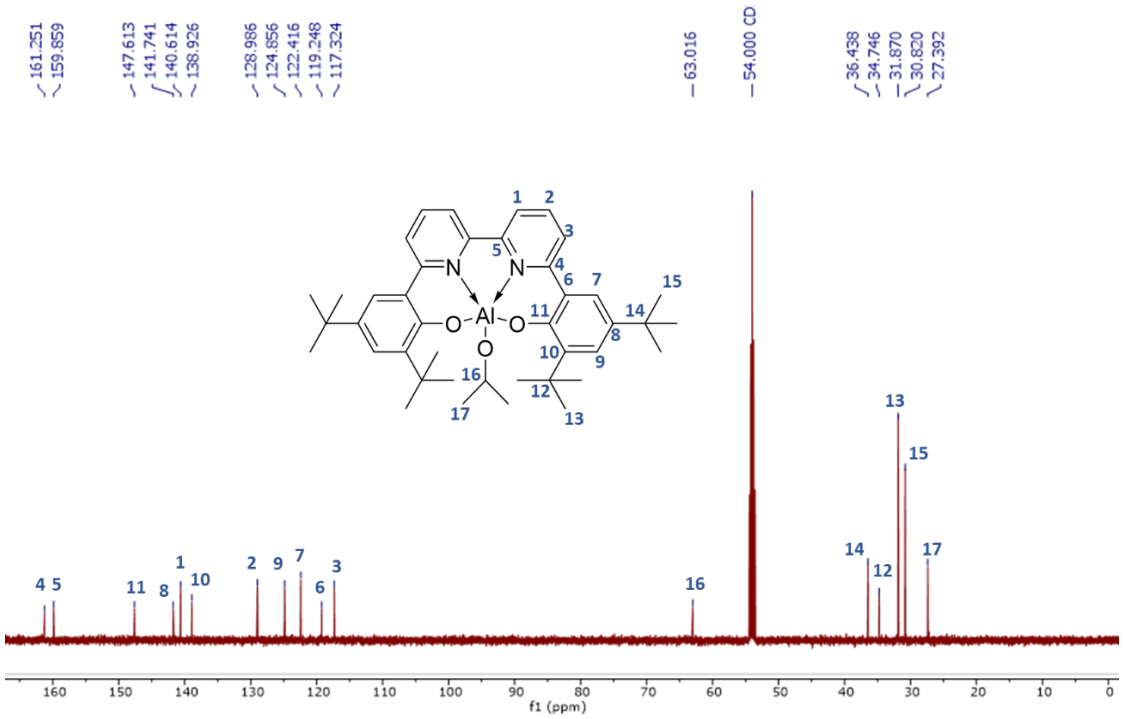

Figure S8. $^{13}C\{^{1}H\}$ NMR spectrum of ($^{t\text{-Bu}}$dhbpy)AlO^{i}Pr (CD_2Cl_2; 126 MHz) with assignments indicated.

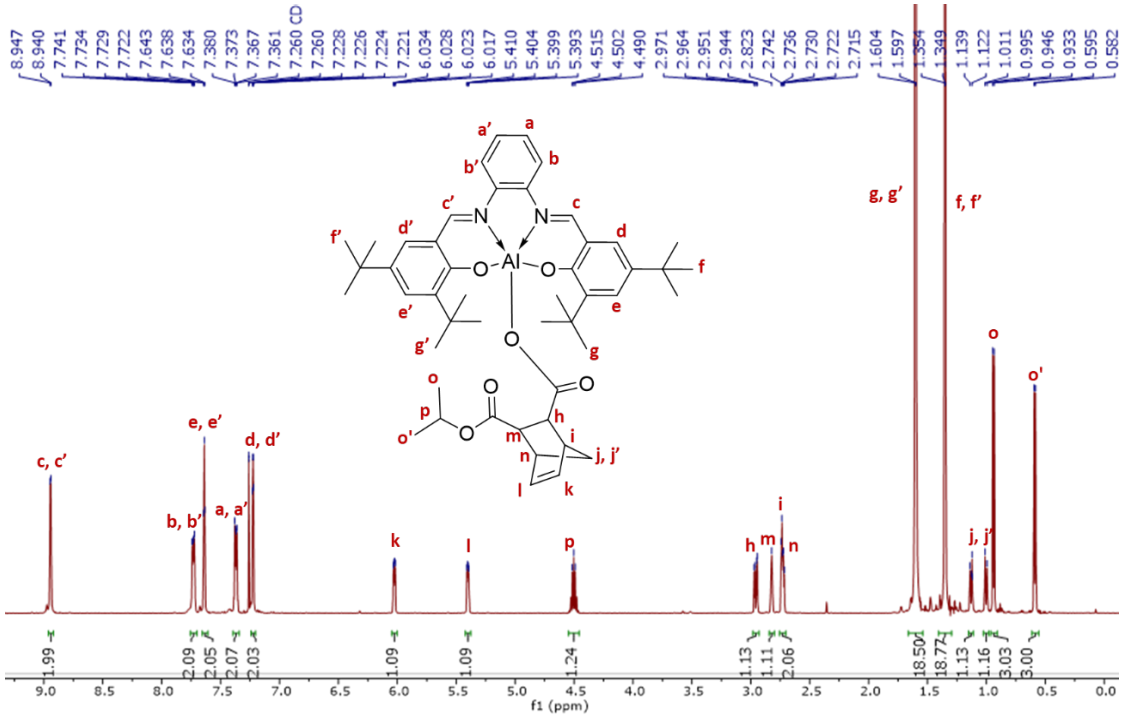

Figure S9. ^{1}H NMR spectrum of ($^{t\text{-Bu}}$salph)Al(oCPMA) ($CDCl_3$; 500 MHz) with assignments indicated.

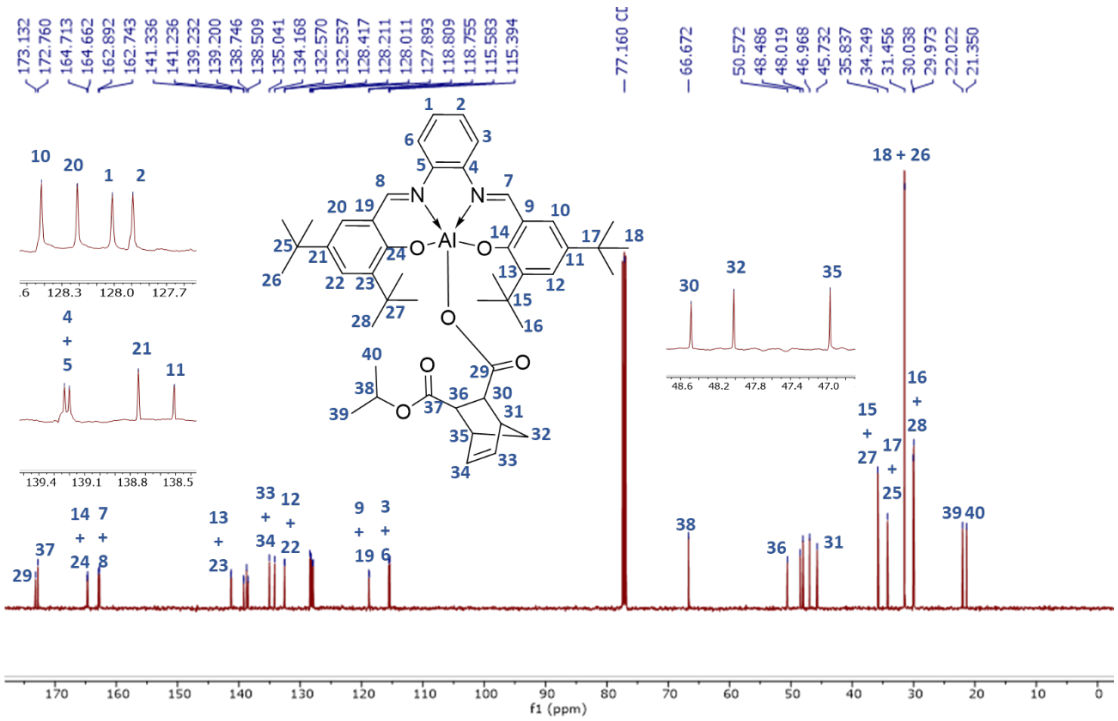

Figure S10. $^{13}C\{^{1}H\}$ NMR spectrum of ($^{t\text{-Bu}}$salph)Al(oCPMA) ($CDCl_3$; 126 MHz) with assignments indicated.

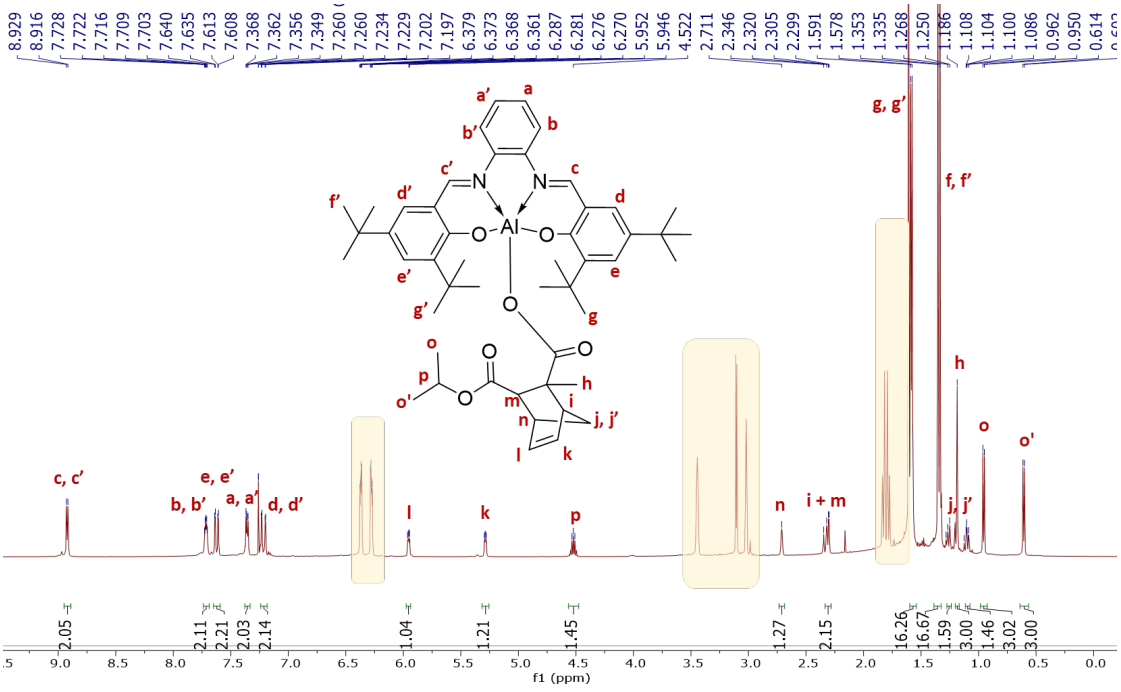

Figure S11. ^{1}H NMR spectrum of the ring-opening of CPCA (5 eq) by ($^{t\text{-Bu}}$salph)AlO^{i}Pr ($CDCl_3$; 500 MHz); signals of excess CPCA are highlighted in yellow and peak assignments are indicated.

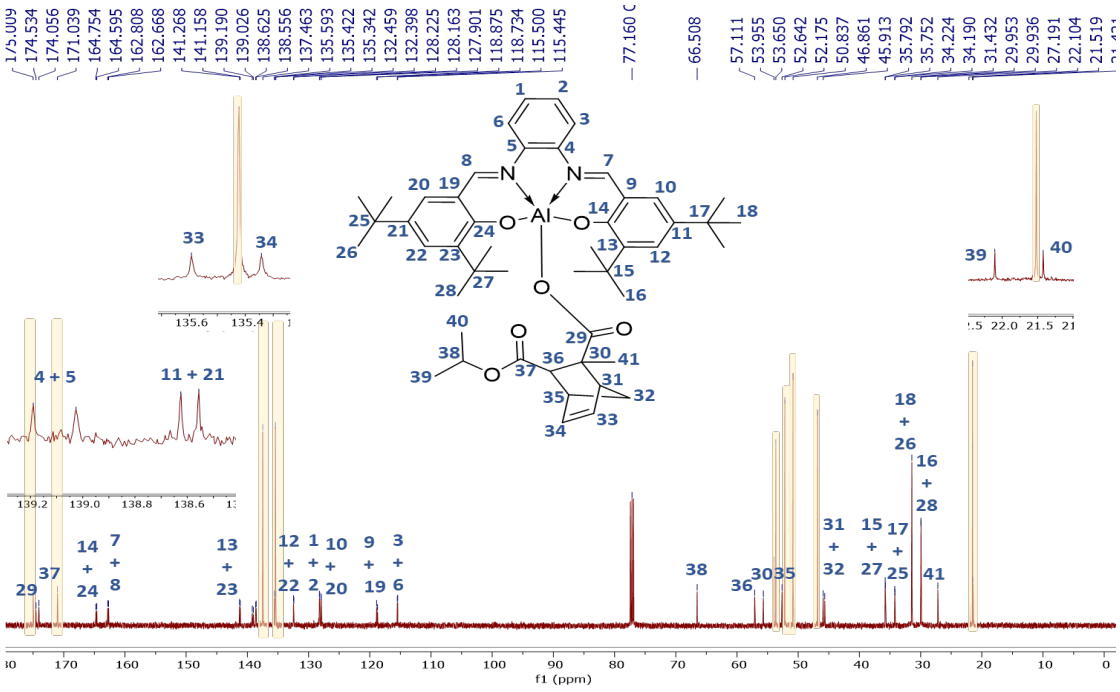

Figure S12. $^{13}C\{^{1}H\}$ NMR spectrum of the ring-opening of CPCA (5 eq) by ($^{t\text{-Bu}}$salph)AlO^{i}Pr ($CDCl_3$; 126 MHz); signals of excess CPCA are highlighted in yellow and peak assignments are indicated.

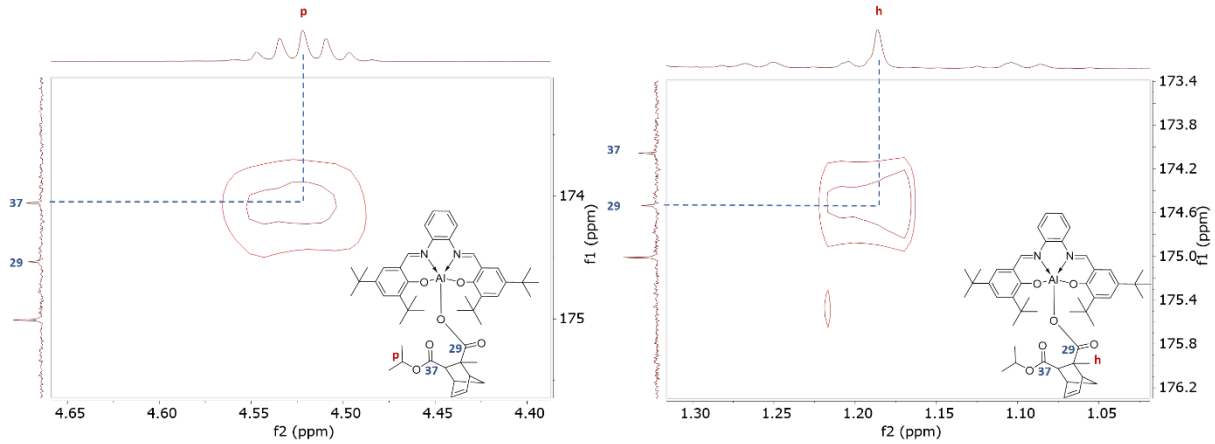

Figure S13. Expansion of the carbonyl region in the ^{1}H-^{13}C HMBC spectrum of the ring-opening of CPCA (5 eq) by ($^{t\text{-Bu}}$salph)AlO^{i}Pr ($CDCl_3$; 500 MHz) showing correlations between the isopropyl methine proton and the distal carbonyl carbon (*left*) and the methyl protons and the proximal carbonyl carbon (*right*).

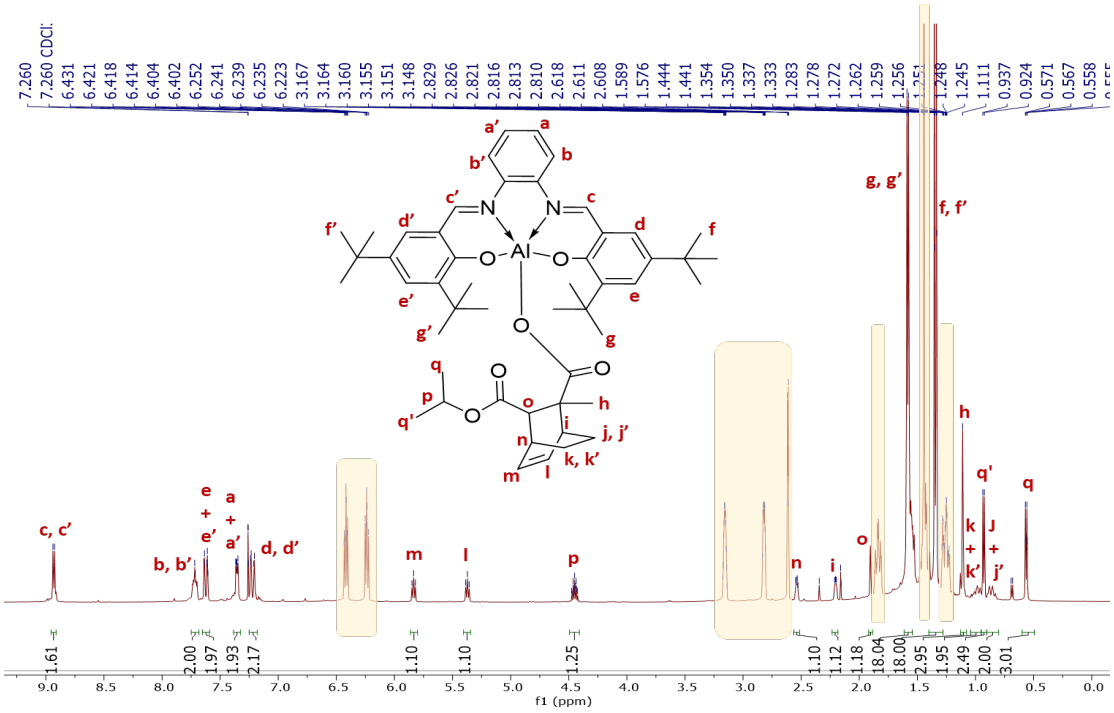

Figure S14. ^{1}H NMR spectrum of the ring-opening of CHCA (5 eq) by ($^{t\text{-Bu}}$salph)AlO^{i}Pr ($CDCl_3$; 500 MHz); signals of excess CHCA are highlighted in yellow and peak assignments are indicated.

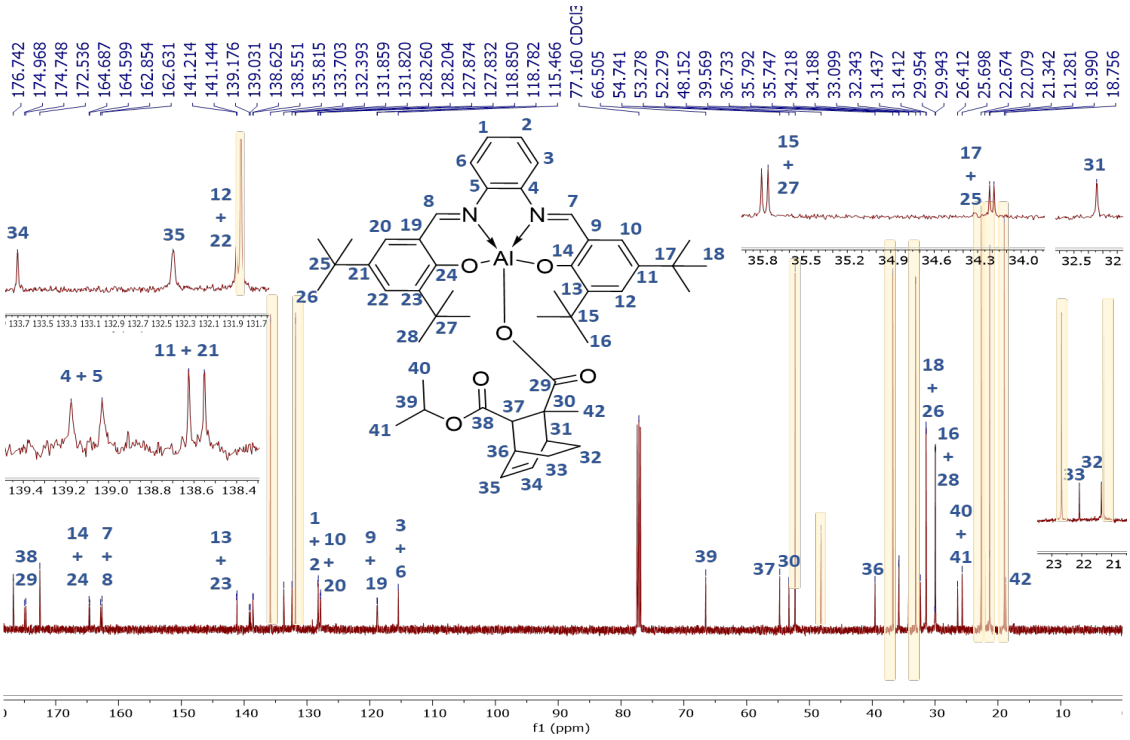

Figure S15. $^{13}C\{^{1}H\}$ NMR spectrum of the ring-opening of CHCA (5 eq) by ($^{t\text{-Bu}}$salph)AlO^{i}Pr ($CDCl_3$; 126 MHz); signals of excess CHCA are highlighted yellow and peak assignments are indicated.

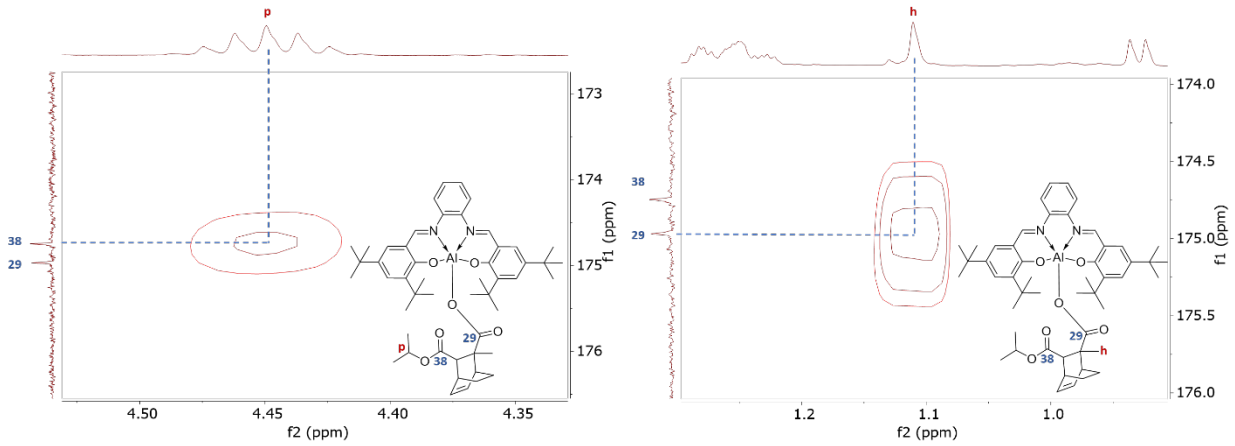

Figure S16. Expansion of the carbonyl region in the ^{1}H-^{13}C HMBC spectrum of the ring-opening of CPCA (5 eq) by ($^{t\text{-Bu}}$salph)AlO^{i}Pr ($CDCl_3$; 500 MHz) showing correlations between the isopropyl methine proton and the distal carbonyl carbon (*left*) and the methyl protons and the proximal carbonyl carbon (*right*).

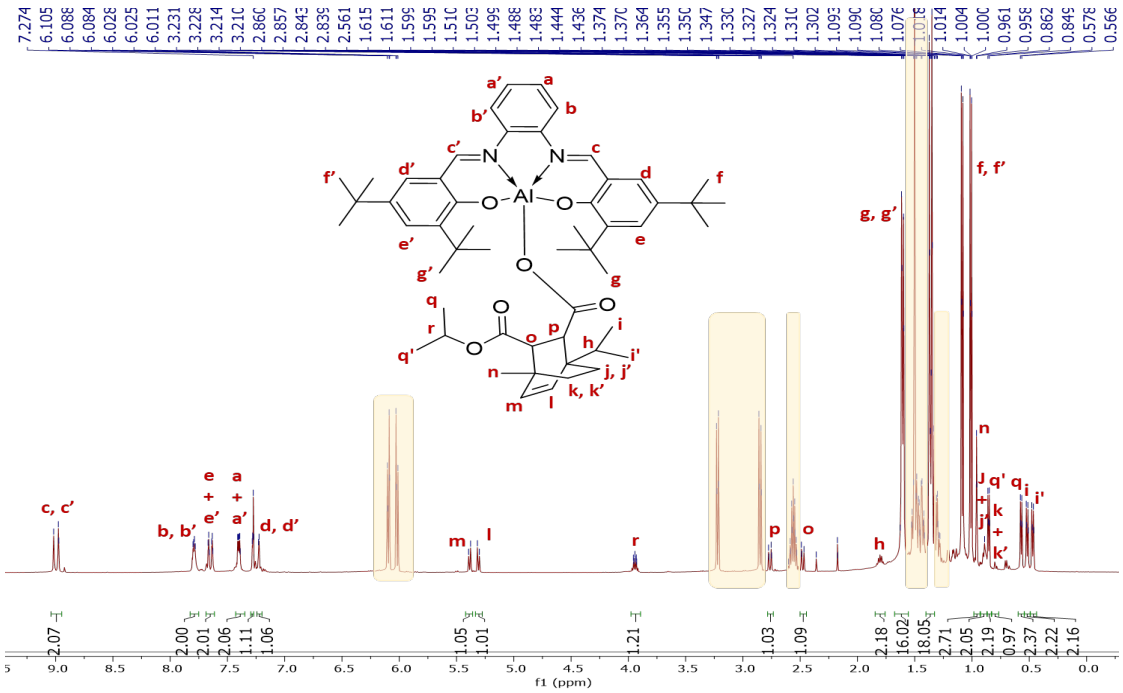

Figure S17. ^{1}H NMR spectrum of the ring-opening of TPMA (5 eq) by ($^{t\text{-Bu}}$salph)AlO^{i}Pr ($CDCl_3$; 500 MHz); signals of excess TPMA are highlighted in yellow and peak assignments are indicated.

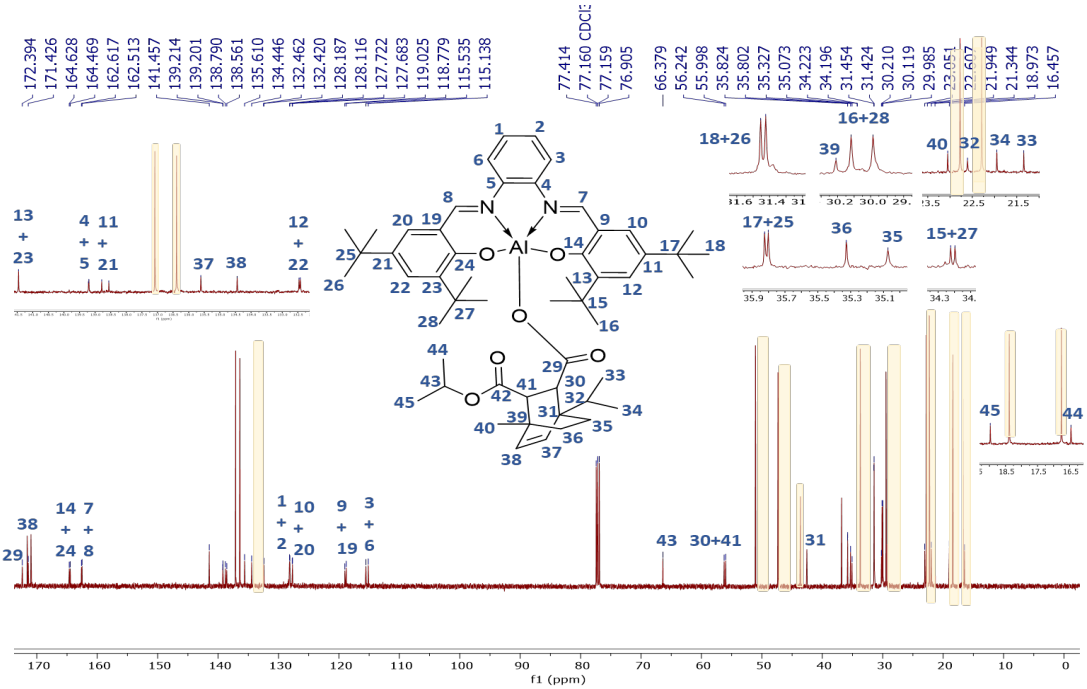

Figure S18. $^{13}C\{^{1}H\}$ NMR spectrum of the ring-opening of TPMA (5 eq) by ($^{t\text{-Bu}}$salph)AlO^{i}Pr ($CDCl_3$; 126 MHz); signals of excess TPMA are highlighted yellow and peak assignments are indicated.

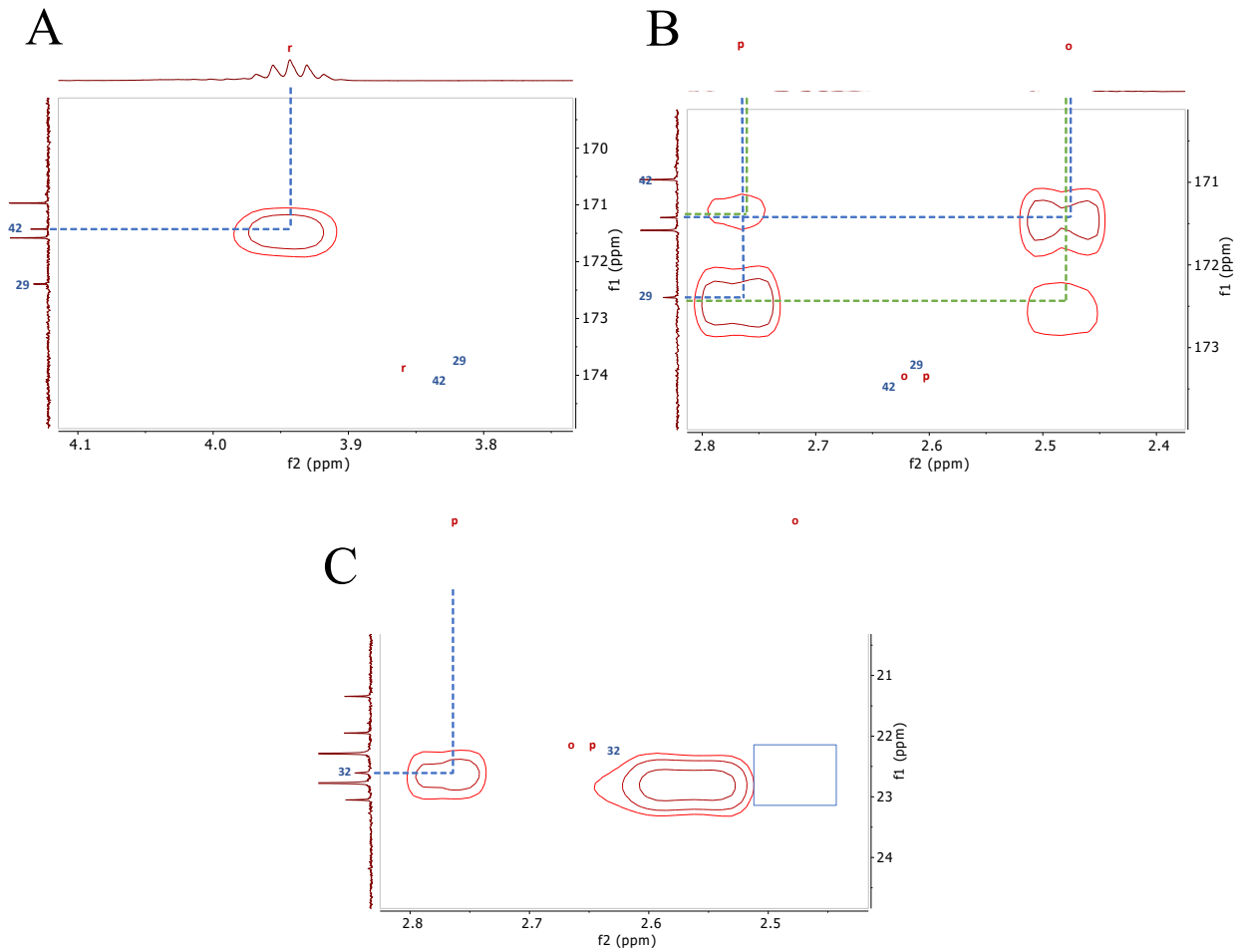

Figure S19. Expansion of the ^{1}H-^{13}C HMBC spectrum of the ring-opening of TPMA (5 eq) by ($^{t\text{-}Bu}$salph)AlO^{i}Pr ($CDCl_3$; 500 MHz) showing correlations between the isopropyl methine proton and the distal carbonyl carbon; B) Correlation between the two carbonyl carbons and the methine protons alpha to the carbonyl groups ($^{2}J_{C\text{-}H}$ correlations indicated in blue; $^{3}J_{C\text{-}H}$ correlations indicated in green); C) Correlation between the methine proton alpha to the proximal carbonyl and the carbon of the isopropyl (determined separately by HSQC analysis) and lack of correlation to the distal methine proton alpha to the distal carbonyl (indicated by a blank square).

5. General polymerization procedure

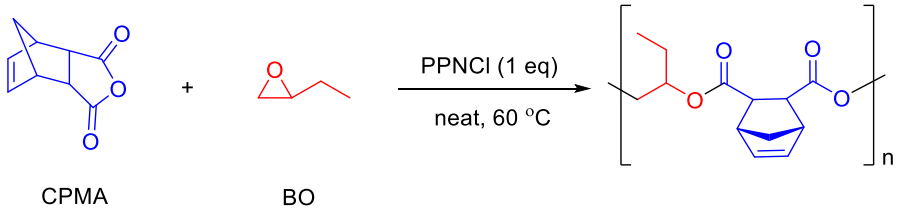

CPMA BO

An aluminum block was pre-heated to 60 °C. In a glovebox, the catalyst (3.8-7.6 µmol, 1 eq.), co-catalyst (PPNCl; 3.8-7.6 µmol, 1 eq.) and CPMA (125 mg, 0.76 mmol, 100-200 eq.) were weighed into a 3 mL vial containing a stir bar. Then, BO (330 µL, 3.82 mmol, 500-100 eq.) was added, the vial was capped with a Teflon-coated screw cap, secured with electrical tape and brought out of the box. The vial was placed in the block and left to stir for 1-2 h (see Table 1) before quenching the reaction by cooling to room temperature and opening to air. Subsequently, an aliquot was dissolved in $CDCl_3$ and analyzed by ^1H NMR spectroscopy to determine the conversion (Table 1). The results displayed relatively broad conversion ranges for some of the polymerizations which were attributed to variations in initial catalyst/co-catalyst/anhydride ratios resulting from issues related to weighing small amounts of material in the glove box and performing the polymerization under neat conditions, thus preventing the use of stock solutions.

6. Stoichiometric reactions of CPMA ring-opening monitored by NMR spectroscopy

In a glovebox the catalyst (20.1 µmol, 1 eq.) and CPMA (3.31 mg, 20.1 µmol, 1 eq.) were weighed into a 3 mL vial and dissolved in 500 µl of $CDCl_3$ to obtain a 0.04 M solution. Then, the solution was transferred into a J-Young tube, the tube was sealed and brought out of the box. A ^1H NMR spectrum of the reaction mixture was recorded at room temperature prior to ring-opening to validate the initial stoichiometry. Then the tube was placed in a pre-heated (60 °C) bath. Upon reaching 1, 3, 5, 7 and 22 h time points the

tube was removed from the bath, analyzed by ^{1}H NMR spectroscopy to determine the conversion and placed in the bath again.

Ring-opening of the anhydride was indicated by the formation of three new signals assigned to the ring-opened product (2.84-2.64 ppm) due to the loss of symmetry upon ring-opening and coordination to the metal center, as well as the concomitant formation of two signals at 0.90 and 0.57 ppm assigned to the isopropyl group. Conversions were calculated from the ratio between the signals of CPMA (3.57 and 3.51 ppm) and ring-open product (2.96 and 2.82 ppm), and represent the average of triplicate runs:

Table S1. Average conversion (%) of CPMA ring-opening by the ($^{t\text{-Bu}}$salph)AlO^{i}Pr and ($^{t\text{-Bu}}$dhbpy)AlO^{i}Pr complexes; standard deviations in parentheses.

Time [h]	($^{t\text{-Bu}}$salph)AlO^{i}Pr	($^{t\text{-Bu}}$dhbpy)AlO^{i}Pr
1 h	8.3 (±0.9)	12.6 (±1.2)
3 h	12.7 (±0.5)	18.0 (±2.2)
5 h	16.3 (±0.5)	21.6 (±4.2)
7 h	21.3 (±0.9)	26.6 (±4.8)
22 h	44.7 (±0.9)	44.3 (±9.5)
48 h	77.3 (±0.5)	73.6 (±3.7)

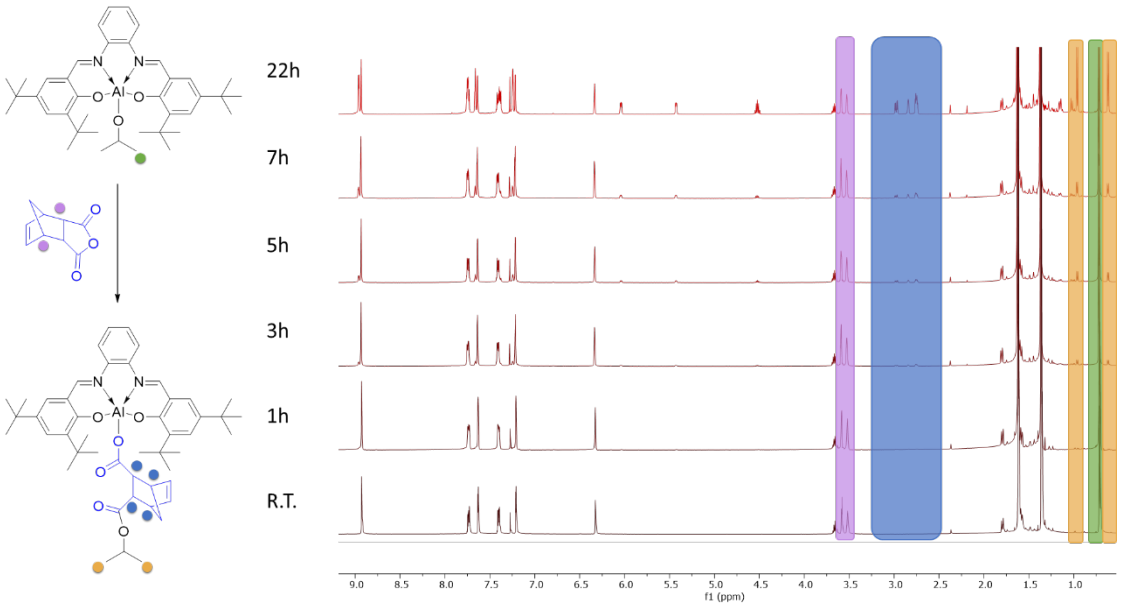

Figure S20. ^{1}H NMR monitoring of the CPMA ring-opening by ($^{t\text{-Bu}}$salph)AlO^{i}Pr.

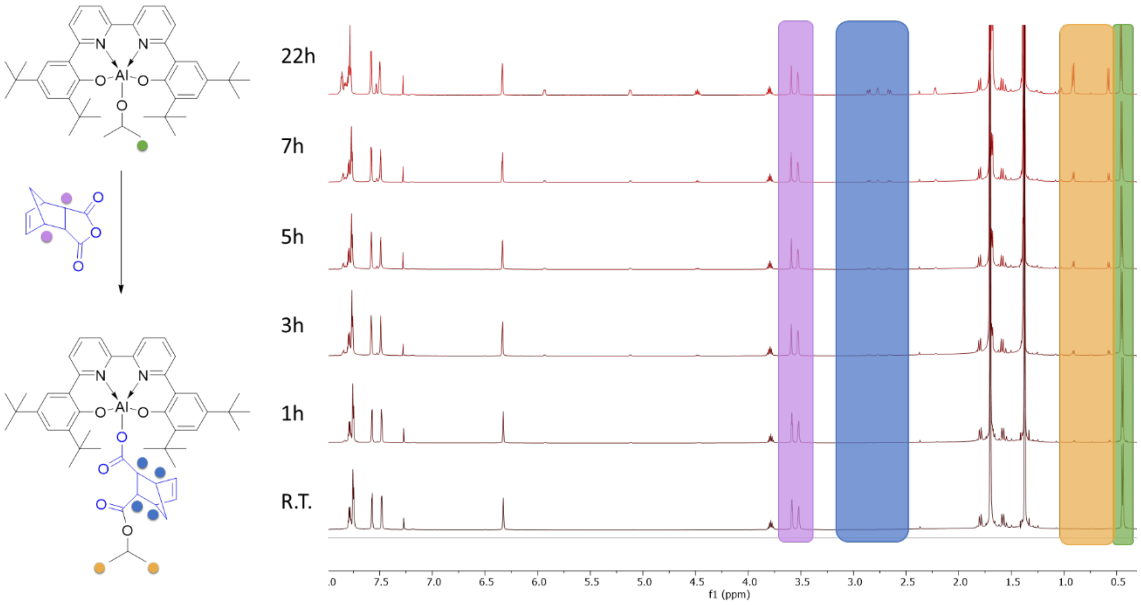

Figure S21. ^{1}H NMR monitoring of CPMA ring-opening by ($^{t\text{-Bu}}$dhbpy)AlO^{i}Pr.

7. Temperature dependence of CPMA ring-opening

The CPMA ring-opening reaction was performed as described above and monitored by ^{1}H NMR spectroscopy using ($^{t\text{-Bu}}$salph)AlO^{i}Pr and dichloroethane (DCE-d_4) as NMR solvent.

Table S2. Conversion (%) of CPMA ring-opening by ($^{t\text{-Bu}}$salph)AlO^{i}Pr at 80 °C using 1 or 30 equivalents of CPMA (0.04-1.2M).

Time [h]	60 °C		80 °C	
	1 eq	30 eq	1 eq	30 eq
1 h	8	24	16	85
3 h	13	38	31	100
5 h	16	51	34	-
7 h	21	63	35	-
22 h	45	94	42	-

8. Kinetics measurements of CPMA ring-opening by NMR spectroscopy

In a glovebox ($^{t\text{-Bu}}$salph)AlO^{i}Pr (12.6 mg, 20.1 μmol, 1 eq.), internal standard [bis(p-trimethylsilyl)benzene], and CPMA were added into a J-Young NMR tube in target concentrations of 0.04, 0.01, and 0.04-1.00 M, respectively, and dissolved in a mixture of 10% DCE-d_4 in DCE at 35 °C (a temperature at which the reaction is not initiated). The tube was brought out of the box and analyzed by ^{1}H NMR spectroscopy at room temperature. Subsequently, the NMR probe was heated to 80 °C (calibrated via a MeOH standard) and the progress of the reactions (performed in triplicate) was monitored for 2 h by acquiring ^{1}H NMR spectral arrays with a relaxation time of 2 s, 100 s delay between experiments (8 scans each) and maximum gain. The obtained arrayed NMR data were phased and baseline corrected in Mestrenova (http://mestrelab.com/) before being integrated. Due to overlaps between signals of CPMA and the NMR solvent, integrations of the imine signals assigned to the starting complex and ring-opened product were used to determine the concentration as a function of time (Figure S13). The integrals were

recorded and entered into an Excel spreadsheet and absolute concentrations of the starting complex as a function of time were computed relative to the concentration of internal standard. Reaction time was calculated in seconds from the known duration per NMR experiment, taking into account the time required for the NMR probe to reach its target temperature from the start of the ^{1}H NMR data acquisition.

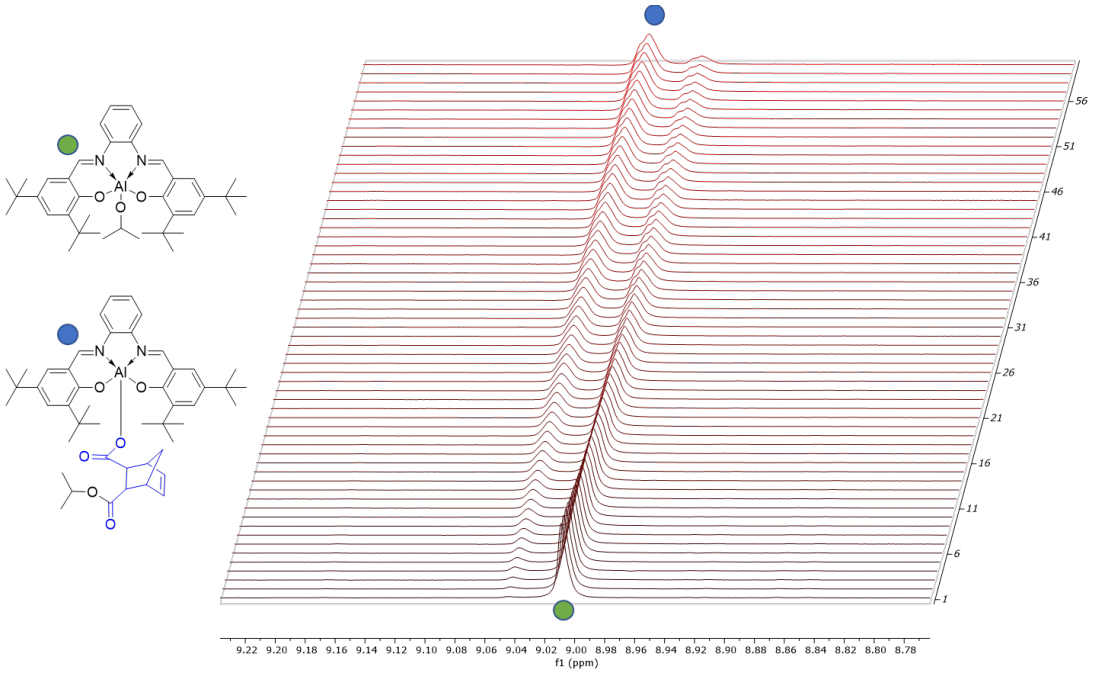

Figure S22. Representative ^{1}H NMR spectra acquired during the ring-opening of CPMA using 30 eq. of the anhydride, showing the growth of ring-open product (9.06 ppm) and the decay of CPMA (9.02 ppm) as a function of time.

9. Kinetic data analysis

A first-order dependence of the rate of reaction on anhydride concentration was determined by good linear correlations between ln[($^{t\text{-Bu}}$salph)AlO^{i}Pr] and time (Figure S23). Due to deviations from linearity at the beginning of the reactions, attributed to the time required for temperature-equilibration in the NMR probe, the kinetic data analyses were performed on a truncated data set wherein the initial time point was selected to be

830 [s]. The observed reaction rate constants (k_{obs}) were calculated from the slopes of the plots of ln[($^{t\text{-Bu}}$salph)AlO^{i}Pr] vs time and the average values are presented in Table S3. The average k_{obs} values were plotted as a function of the experimentally-determined average initial CPMA concentrations (for each equivalent of CPMA employed; Figure S24). This plot showing an increase in rate up to 15 equivalents followed by a decease at high CPMA concentration (20-25 equivalents). A linear fit to the data for up to 15 equiv is shown. A small non-zero y-axis intercept is noted, which suggests the possibility of an additional contribution to the rate law. This deviation might be due to either decomposition of the complex at 80 °C (unlikely, as no decomposition was observed in a control reaction run in the absence of CPMA for 2 h at 80 °C) or a contaminant in the CPMA monomer (e.g. acidic impurity).

Despite a relatively large dispersity in k_{obs} values for the 10 equivalents dataset, the truncated data showing the increase in rate by augmenting the amount of CPMA from 1.1 to 8 equivalents (calculated from the experimentally determined average concentrations of the starting complex and anhydride) were used to calculate a second-order rate constant for the ring-opening of the anhydride. The latter was obtained from the slope of the k_{obs} as a function of initial CPMA concentration by treating the velocity data as *pseudo first-order* kinetics.

Table S3. Summary of kinetic parameters determined by ^{1}H NMR array measurements and fitting of the data with Origin.

Entry	Target initial CPMA conc. [M]	run	Exp. initial CPMA conc. [M]	Avg. initial CPMA conc. [M]	Exp. initial ($^{t\text{-Bu}}$salph)AlO^{i}Pr conc. [M]	Avg. initial ($^{t\text{-Bu}}$salph)AlO^{i}Pr conc. [M]	k_{obs} [s^{-1}]	Avg. k_{obs} [s^{-1}]
1	0.04	1	0.0671	0.05858	0.0514	0.05505	1.4533E-5	1.5238E-05
2		2	0.0518		0.0601		1.5192E-5	
3		3	0.0569		0.05365		1.5988E-5	
4	0.2	1	0.1581	0.1404	0.0567	0.055867	3.1983E-5	3.6561E-05
5		2	0.1295		0.0603		4.0302E-5	
6		3	0.1337		0.0506		3.7397E-5	
7	0.4	1	0.2895	0.2896	0.0502	0.05155	3.0801E-5	4.2039E-05
8		2	0.2889		0.05435		3.5984E-5	
9		3	0.2905		0.0501		5.9331E-5	
10	0.6	1	0.4801	0.4721	0.05695	0.0589	6.2774E-5	5.9596E-05
11		2	0.4651		0.06385		5.2013E-5	
12		3	0.4711		0.0559		6.4000E-5	
13	0.8	1	0.5862	0.5644	0.06095	0.056917	5.7202E-5	4.8223E-05
14		2	0.5895		0.05735		3.8512E-5	
15		3	0.5174		0.05245		4.8956E-5	
16	1	1	0.5627	0.7054	0.05265	0.05605	4.7500E-5	4.9361E-05
17		2	0.7992		0.05625		6.3488E-5	
18		3	0.7544		0.05925		3.7096E-5	

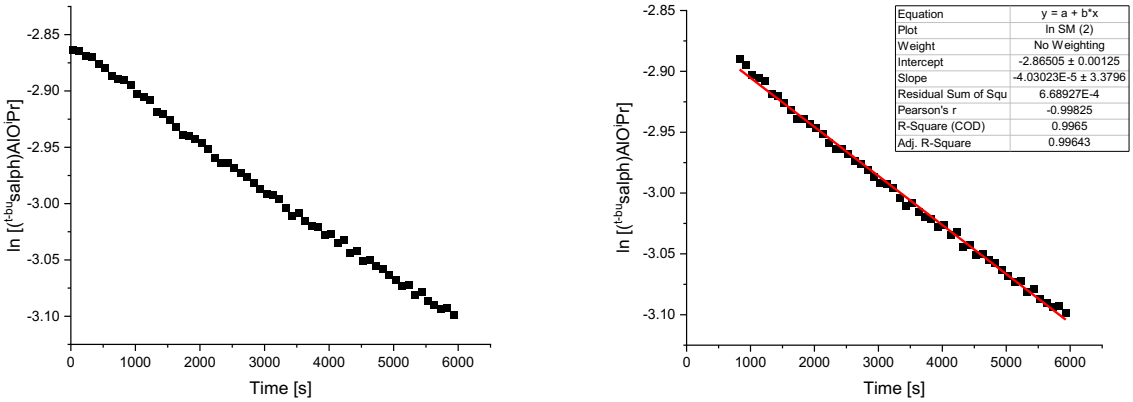

Figure S23. Representative plots of [($^{t\text{-Bu}}$salph)AlO^{i}Pr] decay as a function of time determined from the ^{1}H NMR imine resonance of [($^{t\text{-Bu}}$salph)AlO^{i}Pr] during the ring-opening with5 equivalents of CPMA at 80 °C. Linear fit was determined with Origin using a truncated set (right spectrum) wherein 830 [s] was selected as the initial time point after temperature equilibration in the NMR probe.

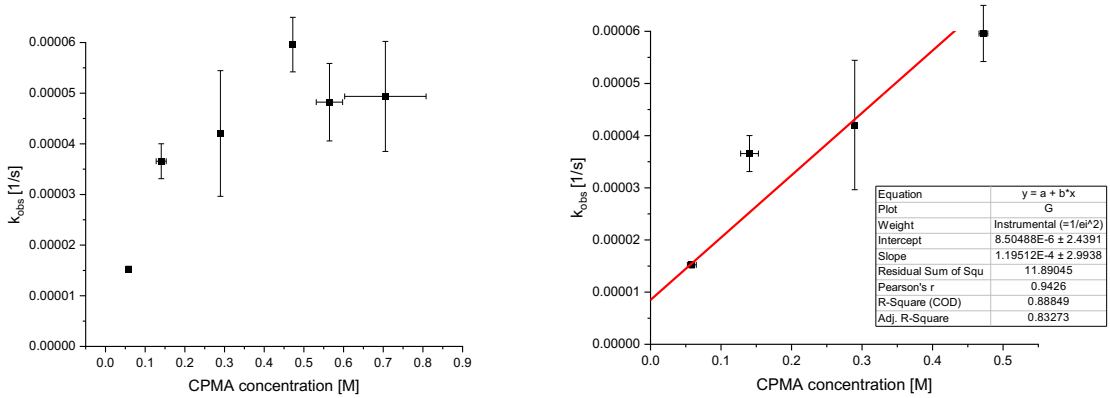

Figure S24. Plots of the average k_{obs} values calculated for the ring-opening of 1, 5, 10, 15, 20 and 25 equivalents of CPMA as a function of the average concentration of CPMA, showing an increase in rate up to 15 equivalents and a decrease at high concentrations of CPMA (*right*); and calculation of the second-order rate constant from the slope of the truncated data set showing increase in rate in augmenting the equivalents of CPMA from 5 to 15 (*left*).

10. Evaluation of equilibrium in the ring-opening process

In a glovebox ($^{t\text{-Bu}}$salph)Al(oCPMA) (10 mg, 12.7 μmol, 1 eq.), internal standard [bis(p-trimethylsilyl)benzene] (0.005 M), and CPCA (2.3 mg, 12.7 μmol, 1 eq.) were added into two J-Young NMR tubes. To one of the tubes,PPNCl (7.3 mg, 12.7 μmol, 1 eq.) was added and the mixtures were dissolved in $CDCl_3$ (0.5 mL). The tubes were brought out of the box, analyzed by ^{1}H NMR at R.T. and placed in a pre-heated oil bath at 60 °C. NMR spectra were recorded after 4 and 24 h, as well as after heating at 80 °C for additional 24 h. In both cases the NMR spectrum of the reaction mixture remained unchanged representing the superposition of the NMR spectra assigned to the reactants (Figure S16).

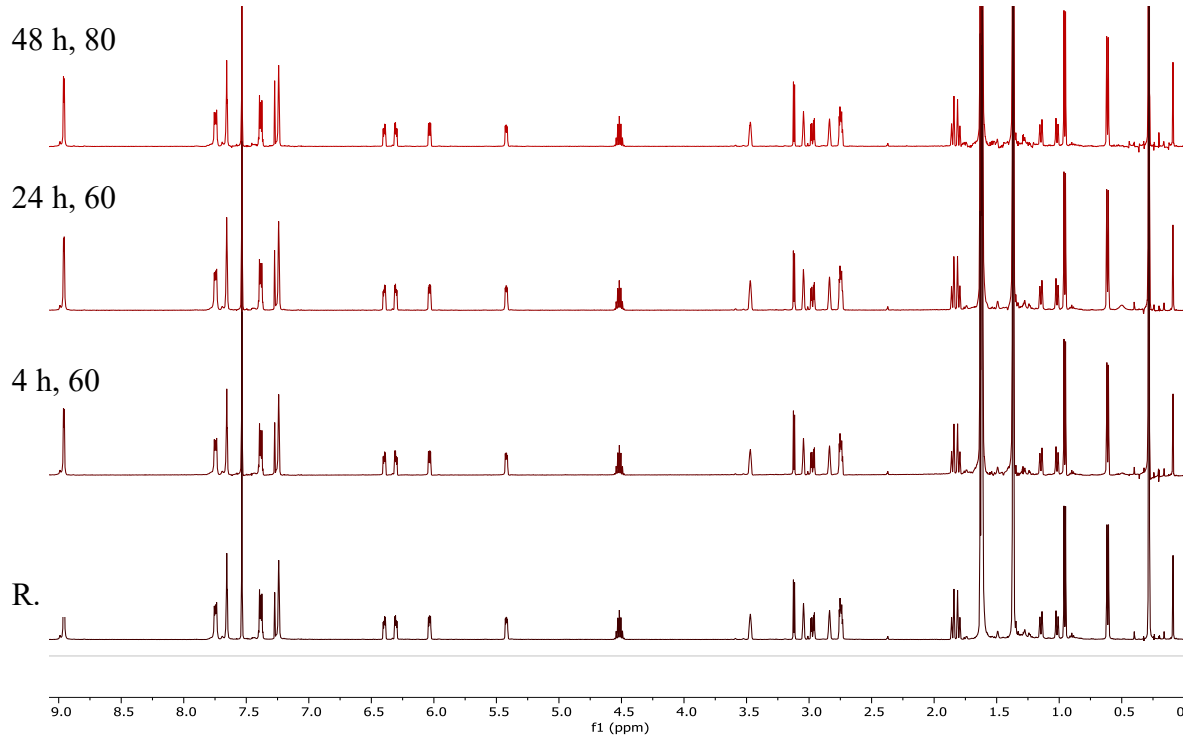

Figure S25. ^{1}H NMR monitoring of the reaction between ($^{t\text{-Bu}}$salph)Al(oCPMA) and CPCA.

11. X-ray crystallography

($^{t\text{-Bu}}$dhbpy)AlCl (CCDC deposition number 2024016): Two level B alerts were generated in the CheckCif: the first alert indicated there was unaccounted electron density and the second alert indicated there was a large Ueq for two carbon atoms. Both of these alerts arise from small components of disorder that were not modeled and do not impact the structure or analysis. The alerts are due to a disordered chlorine atom in a DCM molecule and a disordered t-butyl substituent on the ligand, respectively.

($^{t\text{-Bu}}$dhbpy)Al(oCPMA-O^{i}Pr) (CCDC deposition number 2024019): The crystal quality was poor and diffracted weakly at resolutions greater than 1.5 Å. The quality of the data has led us to analyze this structure only for connectivity purposes. The refinement required the SWAT instruction to model solvent disorder.

($^{t\text{-Bu}}$salph)Al(oCPCA-OiPr) (CCDC deposition number 2024017): The crystal was a pseudo-merohedral twin with disorder in a solvent molecule, the supporting salph ligand, and in the residual Al material. The structure also has low C-C bond precision due to low resolution data. The various issues with the crystal led us to only analyze the connectivity, and did not enable us to distinguish between the enantiomers formed upon anhydride ring-opening. The crystal was refined as a two-component inversion twin. PLATON SQUEEZE[13] was used to model diffused solvent molecule contribution. EADP constraint as well as, DFIX, SADI, SIMU, and RIGU restraints were used to model disordered atoms.

($^{t\text{-Bu}}$salph)Al(oCHCA-OiPr) (CCDC deposition number 2024018): The crystal was a pseudo-merohedral twin with disorder in a solvent molecule, the supporting salph ligand, and in the residual Al material. The structure also has low C-C bond precision due to low

resolution data. The various issues with the crystal led us to only analyze the connectivity, and did not enable us to distinguish between the enantiomers formed upon anhydride ring-opening. The crystal was determined to be a pseudo-merohedral twin and was refined as a two-component inversion twin. PLATON SQUEEZE[13] was used to model diffused solvent molecule contribution. EADP constraint as well as, DFIX, SAME, and SADI restraints were used to model disordered atoms.

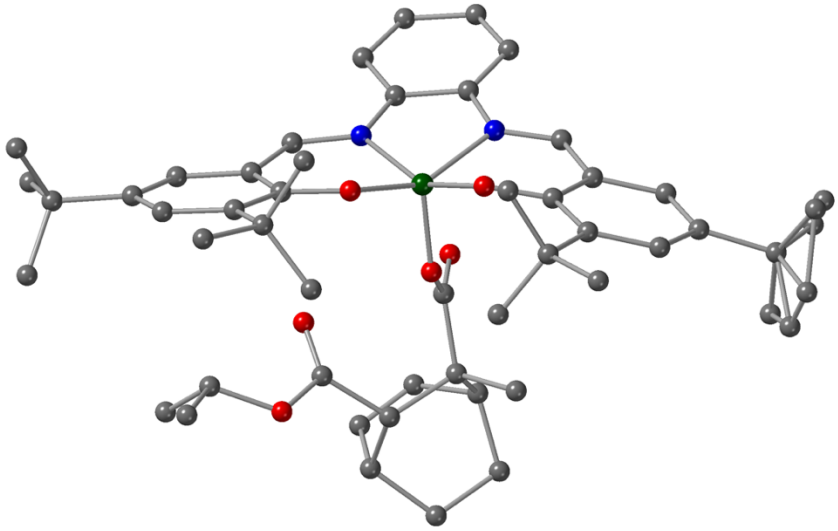

Figure S26. Representation of the X-ray crystal structure of (salph)Al(oCHCA-OiPr), showing all nonhydrogen atoms as isotropic spheres (green = Al, blue = N, red = O, gray = C).

12. References

1 Citron, C. A.; Wickel, S. M.; Schulz, B.; Draeger, S.; Dickschat, J. S. A Diels–Alder/Retro-Diels–Alder Approach for the Enantioselective Synthesis of Microbial Butenolides. *Eur. J. Org. Chem*. **2012**, 6636-6646.

2 Sanford, M. J.; Peña Carrodeguas, L.; Van Zee, N. J.; Kleij, A. W.; Coates, G. W. Alternating Copolymerization of Propylene Oxide and Cyclohexene Oxide with Tricyclic Anhydrides: Access to Partially Renewable Aliphatic Polyesters with High Glass Transition Temperatures. *Macromolecules* **2016**, *49*, 6394−6400.

3 Van Zee, N. J.; Coates, G. W. Alternating Copolymerization of Propylene Oxide with Biorenewable Terpene-Based Cyclic Anhydrides: A Sustainable Route to Aliphatic Polyesters with High Glass Transition Temperatures. *Angew. Chem., Int. Ed*. **2015**, *54*, 2665-2668.

4 Nichols, A. W.; Chatterjee, S.; Sabat, M.; Machan, C. W. Electrocatalytic Reduction of CO_2 to Formate by an Iron Schiff Base Complex. *Inorg. Chem*., **2018**, *57*, 2111−2121.

5 Hooe, S. L.; Dressel, J. M.; Dickie, D. A.; Machan, C. W. Highly Efficient Electrocatalytic Reduction of CO2 to CO by a Molecular Chromium Complex. *ACS Catal*., **2020**, *10*, 1146–1151.
6 Rutherford, D.; Atwood, D. A. Five-Coordinate Aluminum Amides. *Organometallics* **1996**, *15*, 4417-4422.
7 Fieser, M. E.; Sanford, M. J.; Mitchell, L. A.; Dunbar, C. R.; Mandal, M.; Van Zee, N. J.; Urness, D. M.; Cramer, C. J.; Coates, G. W.; Tolman, W. B. Mechanistic Insights into the Alternating Copolymerization of Epoxides and Cyclic Anhydrides Using a (Salph)AlCl and Iminium Salt Catalytic System. *J. Am. Chem. Soc*. **2017**, *139*, 15222–15231.
8 Bruker Analytical X-Ray, Madison, WI, 2016.
9 Sheldrick, G. M., "SHELXT – Integrated space-group and crystal structure determination," *Acta. Cryst*. **2015**, *A71*, 3–8.
10 Sheldrick, G. M., "A short history of SHELX," *Acta. Cryst*. **2008**, *A64*, 112–122.
11 Dolomanov, O.V.; Bourhis, L.J.; Gildea, R.J.; Howard, J.A.K.; Puschmann, H., "OLEX2: A complete structure solution, refinement and analysis program," *J. Appl. Cryst*. **2009**, *42*, 339–341.
12 Hubschle, C. B.; Sheldrick, G. M.; Dittrich, B., "ShelXle: a Qt graphical interface for SHELXL," *J. Appl. Cryst*. **2011**, *44*, 1281–1284.
13 Spek, A. L., "PLATON SQUEEZE: a tool for the calculation of the disordered solvent contribution to the calculated structure factors," *Acta Cryst*. **2015**, *C71*, 9-18.